Performance Analysis of the G^0 Scintillation Detectors

A thesis submitted in partial fulfillment of the requirement
for the degree of Bachelor of Science with Honors in
Physics from the College of William and Mary in Virginia.

by

Stephanie-Louise Bailey

Accepted for _____
(Honors, High Honors, or Highest Honors)

_____
Advisor: Professor David Armstrong

_____
Professor Keith Griffioen

_____
Professor Bill Cooke

_____
Professor Rowan Lockwood

Williamsburg, Virginia
May 2002

Contents

List of Figures

List of Tables

Performance Analysis of the G^0 Scintillation Detectors

Stephanie-Louise Bailey
College of William and Mary

May 2002

Abstract

The G^0 collaboration at Jefferson Laboratory will investigate the contributions of the strange quarks to the fundamental properties of the nucleon by measuring parity-violating electron scattering asymmetries from the proton at both forward and backward angles. The G^0 detector is composed of eight octants of scintillators. Their performance is essential to the G^0 experiment. The overall goal of this thesis was to demonstrate that the detectors' performance is well understood, stable with time, and adequate for the needs of a precision parity-violation experiment. Analysis/software tools were developed to monitor the performance of the detectors. Studies were done using cosmic rays and light emitting diodes.

Acknowledgements

Gibbons who both passed away in 2000. You are always in my thoughts and forever in my heart.

1 Introduction

Spin is a fundamental property of nature like electrical charge or mass. Spin comes in multiples of ½, measured in units of $\hbar$, and can have a positive or negative projection on a given quantization axis. Quarks have spin ½, gluons have spin 1, and the nucleon itself has spin ½. The nucleon refers to the proton and neutron which are the fundamental components of atomic nuclei. Recent experimental evidence indicates that the spin of the nucleon cannot be reproduced from the sum of the spin of the three valence quarks in the nucleon. This is called the spin crisis. One possible explanation for the spin crisis is that the sea of virtual quark anti-quark pairs contributes substantially to the nucleon's spin. The question then arises: if the quark anti-quark sea contributes significantly to the nucleon spin, do they also contribute to nucleon properties such as the charge and current distributions? Since the nucleon has no net strangeness, any effects attributable to strange quarks must be due to virtual strange anti-strange pairs. To investigate this, two parity-violating electron scattering experiments were commissioned: HAPPEX and SAMPLE.

The strange quark effects on the electromagnetic structure of the nucleon are measured by the form factors G_E^S and G_M^S. As will be discussed below, G_E^S and G_M^S can be extracted from measurements of the asymmetry in an electron scattering experiment. In the Hall A Proton Parity Experiment (HAPPEX), at the Jefferson National Accelerator Facility, parity-violating electron scattering asymmetries were measured at $Q^2=0.477$ GeV^2. The experiment was restricted to forward angle asymmetries; no direct extraction of the G_E^S and G_M^S form factors was possible; rather a linear combination was extracted.

The experimental value of $G_E^S + 0.392\,G_M^S$ obtained is 0.025 ± 0.024 [1]. In the SAMPLE experiment, at the Bates Linear Accelerator Center, parity-violating electron scattering asymmetries were measured at $Q^2=0.1$ GeV^2. The experiment was restricted to backward angles asymmetries. The experimental value of $G_M{}^S$ obtained is 0.14 ± 0.42 [2]. In the G^0 experiment, parity-violating electron scattering asymmetries will be measured in the range $0.1<Q^2<1.0$ GeV^2 at both forward and backward angles [3]. These pairs of measurements will allow the separation of the G_E^S and G_M^S form factors.

In Chapter 2, I discuss the physics relevant to the G^0 experiment. This includes discussions of elementary particles, quantum chromodynamics, electromagnetic and weak interactions, form factors, and parity-violating elastic electron scattering. In Chapter 3, I describe some of the subsystems of the G^0 detector. This includes descriptions of the particle beam, target, magnet, scintillators, photomultiplier tubes, electronics, and software. In Chapter 4, I discuss the types of data used in this thesis for testing the performance of the G^0 scintillators. These data include the cosmic ray self-trigger, light emitting diode, and gain monitoring system. In Chapter 5, I describe data analysis of Octant 7 of the G^0 detector. This includes discussions of the absence of cosmic ray events, histogram tails, crosstalk, and detector degradation. In Chapter 6, I describe cosmic ray analysis. This includes discussions of software triggers, run-to-run variations, high voltages, and trends. Chapter 7 summarizes the important results of the data analysis.

2   Physics of the G^0 Experiment

2.1   Elementary Particles

Elementary particles, the simplest constituents of matter, are classified according to their spin angular momentum. Particles with half integer spin, measured in units of $\hbar$, obey Fermi-Dirac statistics and are called fermions. In the Fermi-Dirac case, the wave function is antisymmetric under interchange of two particles. There exists no state for which two or more particles are in the same single-particle state. This is the Pauli-exclusion principle. Particles with integral spin, measured in units of $\hbar$, obey Bose-Einstein statistics and are called bosons. In the Bose-Einstein case, the wave function is symmetric under interchange of two particles. There is no restriction on how many particles can be in any one single-particle state.

Current evidence indicates that matter is composed of two types of fundamental fermions, called quarks and leptons. Quarks and leptons are structureless and point-like on a scale of 10^{-17} m [4]. Quarks occur in six flavors: up (u), down (d), strange (s), charm (c), top (t), and bottom (b). The up, charm, and top quarks carry an electric charge of $\frac{2}{3}e$.

The down, strange and bottom quarks carry an electric charge of $-\frac{1}{3}e$. The up and down quarks are the lightest quarks and have approximately the same mass. The strange quark is somewhat more massive than the up and down quarks. The charm, bottom and top quarks, in order of increasing mass, are significantly more massive than the strange quark. Table 2.1 summarizes the flavors, masses, charges, and spins of the quarks [4]. Corresponding to each quark is an antiquark, a particle with the opposite sign of charge.

Table 2.1. Flavors, masses, charges, and spins of the quarks.

Quarks	Flavor	Mass (eV/c^2)	Charge (e)	Spin ($\hbar$)
u	up	5 M	+2/3	½
d	down	7 M	-1/3	½
s	strange	150 M	-1/3	½
c	charmed	1.5 G	+2/3	½
b	bottom	4.8 G	-1/3	½
t	top	176 G	+2/3	½

Quarks do not exist as free particles but in two types of combinations known as hadrons: mesons and baryons. In the simplest picture, mesons consist of one quark and one antiquark while baryons consist of three quarks. These quarks are known as the "valence" quarks. We have

$$\text{mesons} = Q\overline{Q} \tag{2.1}$$

$$\text{baryons} = QQQ, \tag{2.2}$$

where the bar indicates an antiquark. Protons and neutrons are baryons that are comprised of up and down quarks,

$$\text{p (proton)} = uud = (+2/3) + (+2/3) + (-1/3) = +1 \tag{2.3}$$

$$\text{n (neutron)} = udd = (+2/3) + (-1/3) + (-1/3) = 0. \tag{2.4}$$

In the two statements above, the first equals sign indicates baryon composition and the second equals sign indicates the charges of the corresponding quarks. Protons and neutrons have similar strong interactions with other hadrons. They differ essentially only in their mass and electric charge.

In a hadron, strong interactions among the quarks bind them together. The boson responsible for these interactions is the gluon. A gluon is a neutral, flavorless, massless vector particle. Analogous to electric charge, a color charge is carried by both quarks and gluons. Instead of one type of charge, positive and negative, in the electrical case, there are three colors and their anticolors. The three colors are given the arbitrary names red, green and blue. Quarks carry a color, antiquarks carry an anticolor, and gluons carry one color and one anticolor. Baryons contain all three colors such that they are overall white or colorless. Likewise, mesons contain color-anticolor combinations such that they are colorless. (Note: color charge has nothing to do with optical color.)

In addition to the three valence quarks inside the proton or neutron, there is a "sea" of virtual quarks that originates from the gluons. A virtual particle exists for only a brief instant in an intermediary process in which the conservation of energy appears to be violated. However, one form of the uncertainty principle is

$$\Delta E \Delta t \geq \hbar / 2 . \tag{2.5}$$

According to this relationship, the uncertainty in the energy of a particle multiplied by the uncertainty of time is greater than or equal to $\dfrac{\hbar}{2}$. For a very short time, the uncertainty in the energy can be large. Furthermore, if one sees only the initial decaying particle and the final decay products, one observes that energy is conserved. The virtual particle exists for such a short time that it cannot be directly observed.

The "sea" of virtual quarks in the proton is expected to be made up predominantly of up, down and strange quarks. The heavier quarks are less likely to form since they are significantly more massive. The up and down quarks originating from the gluons are difficult to distinguish from the valence up and down quarks. Thus, the strange quark

provides a unique window on the sea and lends itself to study. Figure 2.1 illustrates the composition of the nucleon as suggested by the theory of the strong interaction. A review of the concepts discussed in the section can be found elsewhere [4].
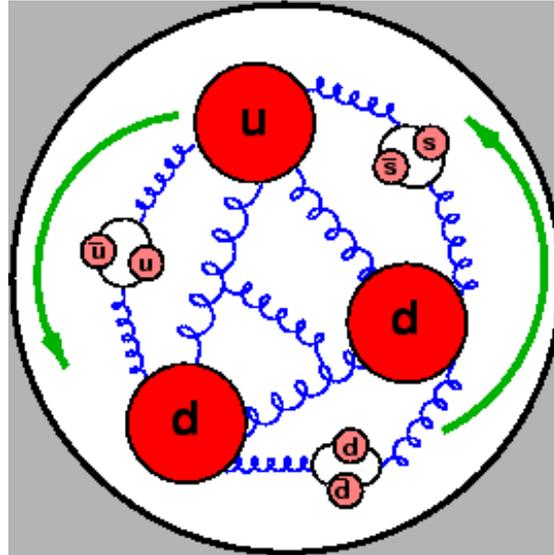
Figure 2.1. The neutron is composed of three valence quarks: one up quark and two down quarks. The large circles represent the valence quarks, wavy lines represent gluons, and small circles represent virtual quark anti-quark pairs.

2.2   Relativistic Kinematics

The relativistic relation between total energy E, 3-momentum $\vec{p}$, and rest mass m of a free particle, in units where c=1, is given by

$$E^2 = p^2 + m^2. \tag{2.6}$$

The Cartesian components of $\vec{p}$, E can be written as components of an energy-momentum 4-vector. The square of the energy-momentum 4-vector is given by

$$Q^2 = \vec{p}^2 + (iE)^2 = p^2 - E^2 = -m^2, \tag{2.7}$$

and is thus invariant. An invariant quantity has the same value in all reference frames.

Similarly, for an elastic scattering process, the 4-momentum transfer squared between the

incident and emergent electron is invariant, with a value

$$
\begin{aligned}
Q^2 &= (\vec{p}_0 - \vec{p})^2 - (E_0 - E)^2 \\
&= (p_0^2 - E_0^2) + (p^2 - E^2) - 2\vec{p}\,\vec{p}_0 + 2E_0 E \\
&= -2m^2 - 2pp_0 \cos\theta + 2E_0 E = 2pp_0(1 - \cos\theta) = 2pp_0 \sin^2\theta,
\end{aligned}
\tag{2.8}
$$

where θ is the angle between the initial and final momentum in the lab frame [5]. The

final step in Equation (2.8) makes the approximation that $m \ll p$, which is valid for high-

energy electrons. Therefore, $m^2 \approx 0$, $p = E$, and $p_0 = E_0$.

2.3 Quantum Chromodynamics

The accepted quantum field theory of electromagnetic interactions is quantum

electrodynamics (QED). In QED the force between two charges is due to photon

exchange and is dominated by a single photon exchange. The coupling constant

specifying the strength of the interaction is the dimensionless fine-structure constant α =

1/137. Thus, the effect due to higher-order terms can be treated by perturbation theory.

The quantum field theory of the strong interaction is called quantum

chromodynamics (QCD). QCD involves the force between colored quarks due to the

exchange of gluons. At all but the highest energies, the interaction between the quarks is

so strong that the idea of a single quantum exchange is inappropriate. The coupling

constant is given by $\alpha_s \cong 4\pi^2$. The main difference lies in that QED involves a neutral

photon, whereas QCD involved a colored gluon. Figure 2.2 illustrates these differences.
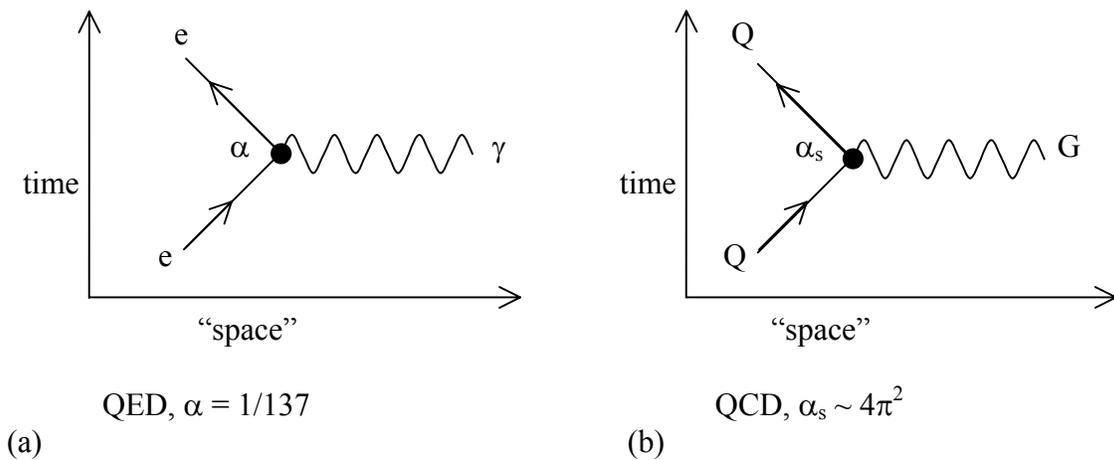
Figure 2.2: Feynman diagram for (a) exchange of photon in Quantum Electrodynamics and (b) exchange of gluon in Quantum Chromodynamics.

Feynman diagrams are pictorial representations of interactions via quantum exchange. In the diagrams above, vertical displacement represents time; a process begins on the bottom and ends on the top. Horizontal displacement indicates particle motion. Every line in the diagram represents a particle. A straight line indicates a particle, and a wavy line represents a photon or gluon. A vertex or a point where three lines meet represents an electromagnetic interaction (interaction due to electric charge) or a strong interaction (due to color). This includes magnetic effects that have to do with moving electric charges.

2.4   Form Factors

The Rutherford formula is a good starting point for discussing charged particle scattering. In Rutherford's experiment, α particles, positively charged nuclei of ^4He atoms, were directed at a thin gold foil and the deflection of the particles were measured as they came out the other side. Figure 2.3 shows a schematic of the Rutherford experiment.
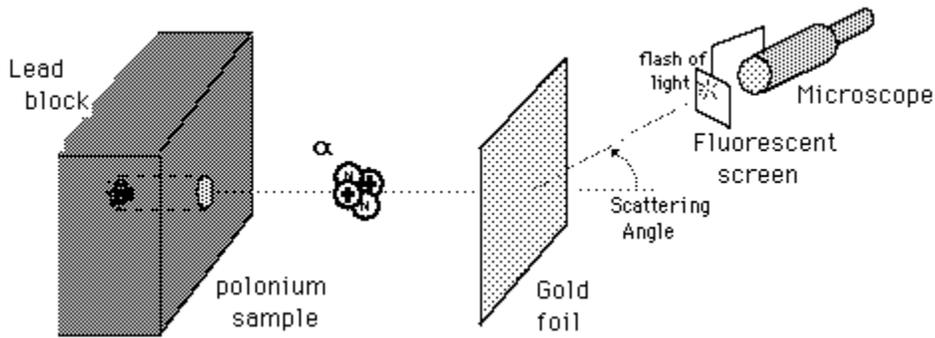
Figure 2.3: Schematic of the Rutherford experiment. Alpha particles from a radioactive source strike a thin gold foil and deflect on the other side. When the alpha particles strike a fluorescent screen, it produces a tiny but visible flash of light.

The Rutherford formula gives the cross-section for elastic scattering of two charged, spinless, point particles due to the electromagnetic interaction. This formula is given by

$$\frac{d\sigma}{d\Omega} = \left\{ \left[\frac{1}{4\pi\varepsilon_0} \right] \frac{zZe^2}{4T\sin^2(\theta/2)} \right\}^2, \qquad (2.9)$$

where z is the charge number of the projectile, equal to 2 for an α particle, Z is the number of protons in the target nucleus, T is the kinetic energy of the α particle, e is the electron charge, ε_0 is the permittivity of vacuum, and θ is the scattering angle. In deriving this expression, Rutherford made several assumptions: (1) relativistic effects are ignored, (2) the target is so massive that it does not significantly recoil, (3) the target is so thin that only a single scattering occurs, (4) the projectile and target particles are so small that they may be treated as point masses and charges, (5) only the Coulomb force is effective, and (6) both projectile and target are spinless.

The electron is a better nuclear probe than the alpha particles of Rutherford scattering because it is a point particle and can easily penetrate the nucleus. For scattering of high-energy electrons and protons, a number of other effects become significant, and the scattering behavior diverges from the Rutherford formula. First, the proton is not infinitely massive and therefore recoils. Second, the probing electrons are relativistic. Third, the proton, being a composite object, is not a point charge but a charge distribution. Fourth, the particles are not spinless and the proton magnetic moment contributes to the interaction.

The cross section for scattering relativistic electrons off point-charged particles is described by the Mott formula and is given by

$$\left(\frac{d\sigma}{d\Omega}\right)_{\text{Point}} = \left\{\left[\frac{1}{4\pi\varepsilon_0}\right]\frac{e^2 ZE}{2p^2 \sin^2(\theta/2)}\right\}\left(1 - \frac{p^2}{E^2}\sin^2\frac{\theta}{2}\right), \qquad (2.10)$$

where p is the magnitude of the momentum and $E = \sqrt{p^2 + m_e^{\ 2}}$ is the total relativistic energy of the incident electron. In the nonrelativistic limit, $E \approx m_e$ and the kinetic energy of the incident electron becomes $T = p^2/2m_e$. This gives the results:

$$\frac{E}{2p^2} \rightarrow \frac{m_e}{2(2m_e T)} = \frac{1}{4T}, \qquad (2.11)$$

and the Mott formula reduces to the Rutherford formula.

The cross-section for scattering by a charge distribution can be written in terms of that for a point target by inclusion of a form factor $F(\vec{q})$

$$\left(\frac{d\sigma}{d\Omega}\right) = \left(\frac{d\sigma}{d\Omega}\right)_{\text{Point}}|F(\vec{q})|^2, \qquad (2.12)$$

where $\vec{q}$ is the momentum transfer from the projectile to the target

$$\vec{q} = \vec{p}_i - \vec{p}_f,$$ (2.13)

and $\vec{p}_i$ and $\vec{p}_f$ are the initial and final momenta. The form factor is the Fourier

transform of the charge distribution

$$F(\vec{q}) = \int \rho(\vec{x}) e^{i\vec{q}\cdot\vec{x}} d^3x.$$ (2.14)

When all of the factors are taken into account, the cross-section is given by

$$\left(\frac{d\sigma}{d\Omega}\right) = \frac{\alpha^2}{4E^2 \sin^4(\theta/2)} \frac{E'}{E} \left[\frac{G_E^2 + \tau G_M^2}{1+\tau} \cos^2\left(\frac{\theta}{2}\right) + 2\tau G_M^2 \sin^2\left(\frac{\theta}{2}\right) \right]$$ (2.15)

where $\tau = -q^2/4m^2$, m is the proton mass, and E' is the new energy of the projectile

after scattering. The G_E and G_M are form factors related to the charge and magnetic

moment distributions in the proton. A review of the concepts discussed in the section can

be found elsewhere [6].

2.5   Electromagnetic and Weak Interactions

An electron and proton can interact via the electromagnetic or the weak force. The

electromagnetic interaction involves the exchange of a virtual photon. Virtual photon

exchange is charge dependent and helicity independent. (The helicity of a particle is its

spin projection along its direction of motion. A particle is called right-handed if its

helicity is positive and left-handed if it is negative.) Weak interactions are responsible for

the decay of massive quarks and leptons to lighter quarks and leptons. The carrier

particles of the weak interactions are the W^+, W^- and the Z bosons. The Z^0 interaction is

charge independent and helicity dependent. Thus, a helicity-dependent (parity-violating)

effect signals the Z^0 exchange. The G^0 form factor is unique in that only through weak

interaction with the proton does the form factor appear. This weak dependence is given by

$$G_E^{P,Z} = \left(\frac{1}{2} - \sin^2 \theta_W\right) G_E^{P,\gamma} - \frac{1}{4} G_E^{0,P}, \tag{2.16}$$

where $G_E^{P,\gamma}$ is the electromagnetic form factor for the proton. The definition of G_E^0 is

$$G_E^{0,P} = \left(\frac{1}{3}\right) \left(G_E^{u,p} + G_E^{d,p} + G_E^{s,p}\right). \tag{2.17}$$

The G_E^0 form factor contains the average of the up, down, and strange quark distributions with the proton. It is a singlet under SU(3) symmetry in which the up, down, and strange quarks have identical strong interactions. The G^0 form factor can be extracted from asymmetry measurements using only proton form factors.

2.5   Parity-violating Elastic Electron Scattering

The probability of scattering is different for positive and negative helicity incident electrons due to the weak interaction. Thus, an accurate determination of this asymmetry will provide a method by which to directly investigate the G^0 form factors. The amplitude of an electron-proton interaction is

$$M = M^\gamma + M^Z, \tag{2.18}$$

where M^γ is the electromagnetic interaction amplitude and M^Z is the weak interaction amplitude. The term M^Z is usually neglected since it is about 10^5 orders of magnitude smaller than M^γ. In quantum mechanics, probabilities are measured rather than amplitudes. Thus the equation becomes

$$|M|^2 = |M^\gamma|^2 + |M^Z|^2 + 2\operatorname{Re}\left(M^\gamma M^Z\right). \tag{2.19}$$

Similarly, the term $\left|M^Z\right|^2$ is negligible. However, M^Z, unlike M^γ, has both vector and axial-vector pieces. In other words, the cross section contains a component that will change signs in the mirror experiment. In parity-violating electron scattering, the mirror measurement is made by reversing the beam helicity. Thus, the cross term in the cross sections violates parity. The cross term can be determined experimentally by comparing the cross sections of the polarized electron beam with positive and negative helicities. Since the parity-violating terms in the cross section are proportional to the electron helicity, the asymmetry is directly related to the cross term

$$A = \frac{\left|M^+\right|^2 - \left|M^-\right|^2}{\left|M^+\right|^2 + \left|M^-\right|^2} \propto \frac{2\,\mathrm{Re}\left[M^Z M^\gamma\right]}{\left|M^\gamma\right|^2}, \tag{2.20}$$

where M^+ are positive helicity interactions and M^- are negative helicity interactions. To experimentally measure M^Z, the scattering probabilities are observed physically as numbers of scattered particles seen by the detector.

$$A = \frac{N^+ - N^-}{N^+ + N^-}, \tag{2.21}$$

where N^+ is the number of scattered particles for positive helicity configurations and N^- is the number of scattered particles for negative helicity configurations. A review of the concepts discussed in the section can be found elsewhere [3].

3 Subsystem Descriptions

3.1 Particle Beam and Target

In this experiment, a beam of electrons is accelerated to high energy by an accelerator (CEBAF at the Thomas Jefferson National Accelerator Facility). The beam of electrons leaves the accelerator and passes into a target. The collisions occur between the electrons in the beam and the material in the target. The target for G^0 is a thin-walled vessel of liquid hydrogen with a diameter of 5 cm and length of 20 cm. The hydrogen atom consists of one electron orbiting around the single proton (which constitutes the nucleus of the hydrogen atom). Most of the time, the electrons will pass through the target without colliding with anything. Occasionally, an electron in the beam will hit a proton in the hydrogen. The case in which the particles scatter elastically (e.g. the proton is not raised to an excited state) is of interest in this experiment.

3.2 Magnet

The spectrometer consists of a toroidal array of eight superconducting coils with a field integral of approximately 1.6 T-m. The spectrometer focuses particles of the same momentum and scattering angle (i.e. with a specific value of Q^2) from the length of the target to a single point in each of the eight octants of the spectrometer.

3.3 Detector Overview

The G^0 detector is composed of eight octants, within a support structure, arranged symmetrically around the beamline axis. Figure 3.1 shows the support structure for the octants. Four of the octants were built by a North American collaboration and the other four were built by a French collaboration. Each octant consists of 16 pairs of arc-shaped plastic scintillators. Each scintillator has two acrylic lightguides, one attached at each

end. Coupled to the ends of each light guide is a photomultiplier tube. Figure 3.2 shows a schematic view of the G^0 Experiment.

Figure 3.1. Support structure for the eight octants. Octant 7 is shown installed in the 12 o'clock position.
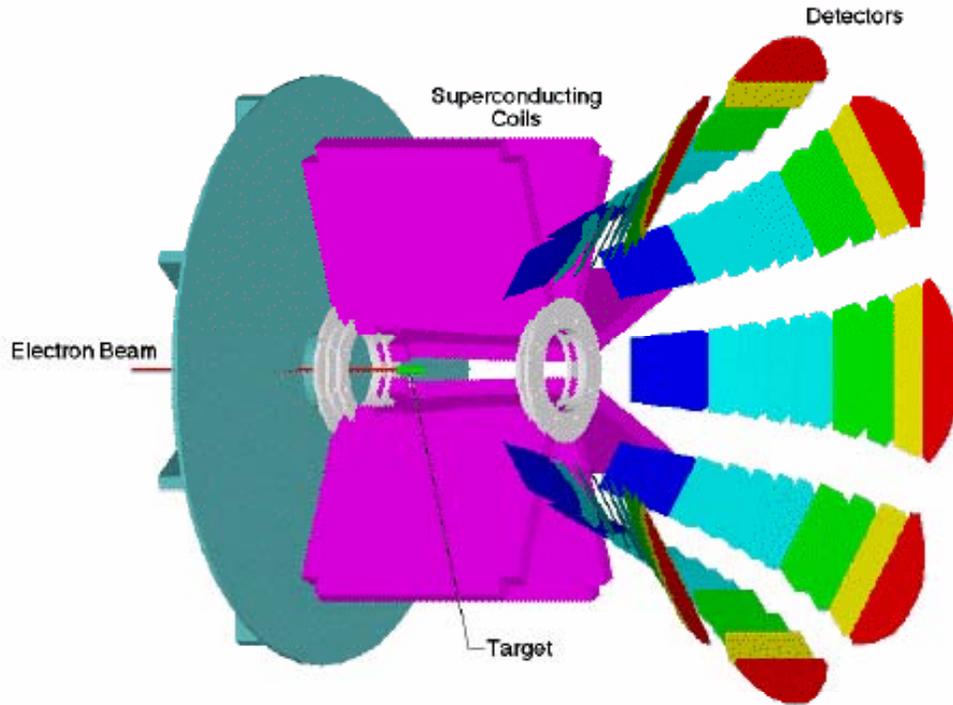
Figure 3.2. Schematic view of the G^0 Experiment showing the spectrometer in the forward angle configuration. Two of the eight coils and one sector of the detectors have been removed for clarity. The spectrometer is comprised of an eight sector superconducting toroidal magnet that focuses recoil protons (forward scattering measurement) or electrons (backward measurement) from a 20 cm long liquid hydrogen to pairs of plastic scintillator detectors.

3.4 Scintillators

The function of scintillators is to detect ionizing radiation. Their performance is essential

to the G^0 experiment. The ideal scintillator should convert a fraction of the deposited

energy of charged particles into detectable light with a high efficiency, convert linearly,

be transparent to the wavelength of its own emission for good light collection, permit

short decay time of the induced luminescence so that fast signal pulses can be generated,

and have an index of refraction near that of glass to allow efficient coupling of the

scintillation light to a photomultiplier tube [7].

Relativistic charged particles lose energy in matter primarily by ionization. Inside a scintillator, a charged particle interacts electromagnetically with atomic electrons and ionizes atoms or molecules in its path. The free electrons subsequently combine with the ions to form neutral pairs that are initially in an excited state. Decay to the ground state produces one or more photons visible or near ultraviolet light, which travel through the scintillator with little attenuation. The production of light happens in about a picosecond.

Each octant in the detector is composed of 16 arc-shaped plastic scintillator pairs (Figure 3.3). The scintillator pairs are numbered 1-16, 1 being the scintillator pair with the shortest length (closest to target) and 16 being the scintillator pair with the longest length (furthest from target). Figure 3.4 shows the numbering of the scintillator pairs in an octant with respect to the target. Each scintillator pair is composed of two identical scintillators[1], one in front and one in back. Each scintillator in the pair has two acrylic light guides, one attached at each end. Coupled to each end of a light guide is a photomultiplier tube, one on the left end of the scintillator and one on the right end of the scintillator. The light guide physically couples the scintillator to the photomultiplier tube and acts as a guide for the scintillation light. So, each scintillator pair has two identical scintillators (front and back), each read out by two photomultiplier tubes (left and right). Each scintillator pair measures a fixed range of Q^2 along its entire length.

---

[1] This is not the case for scintillator pair 4, where the front and back scintillators have a different thickness.

Figure 3.3. An octant comprised of 16 pairs of arc-shaped plastic scintillators. The scintillators are wrapped in aluminized mylar to prevent contaminants such as finger oils from crazing (formation of cracks and scratches) the plastic.
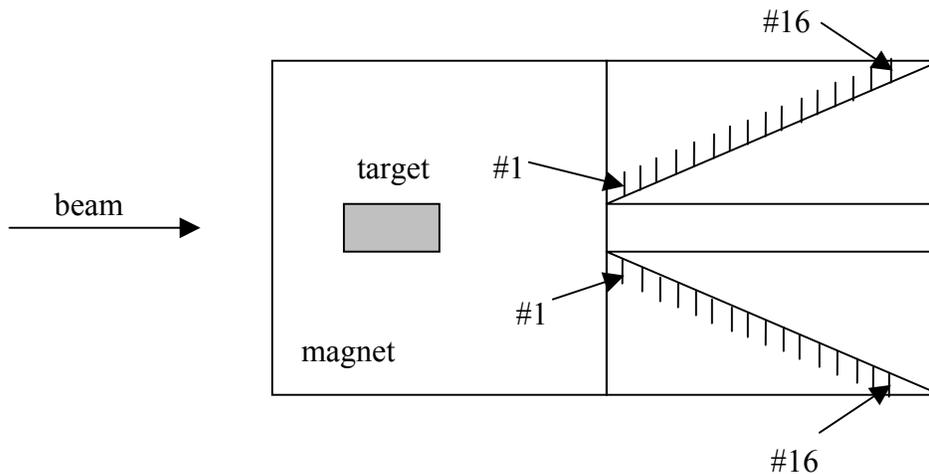
Figure 3.4. A sketch of the cross section of the detector to show the numbering of the scintillator pairs with respect to the target. Octants 1 is shown in the 12 o'clock position and octant 5 is shown in the 6 o'clock position. The other 6 octants are not included in the diagram for clarity. In each octant, scintillator pair 1 is located closest to the target and scintillator pair 16 is located furthest from the detector.

Scintillator thickness varies from pair to pair. In scintillator pairs 1-3, the scintillators are ½ cm thick. In scintillator pair 4, the thickness of the front scintillator is ½ cm and the thickness of the back scintillator is 1 cm. In scintillator pairs 5-16, the scintillators are 1 cm thick. The variation in thickness is due to the size restriction of the octants.

3.5   Photomultiplier Tubes

A photomultiplier tube converts the weak light output of a scintillation pulse, on the order of a few hundred photons, into a corresponding electrical signal. A photomultiplier tube is composed of an outer envelope, a photocathode, and an electron multiplier structure. The outer envelope acts as a pressure boundary to maintain vacuum conditions inside the tube that are required so that low-energy electrons can be accelerated efficiently by internal electric fields. The photocathode converts as many of the incident light photons as possible into low-energy electrons by the photoelectric effect. These electrons are not of sufficient number or energy to be detected by conventional electronics. The electron multiplier serves as an amplifier to increase their number. In the photomultiplier tube, the electrons are attracted to the first dynode by a voltage drop of about 50 volts. The photoelectrons strike the dynode with enough energy to free several new electrons for each photoelectron. The second-generation electrons are, in turn, attracted to the second dynode where a larger third-generation group of electrons are emitted. This process continues for 10 to 12 stages. At the final dynode, enough electrons are available to form a current pulse suitable for further amplification by transistor circuits. The voltage drops between dynodes are established by a single external high voltage. External resistors equalize the voltage drops between the dynodes. Figure 3.5 shows a schematic diagram

of a typical photomultiplier tube. After amplification through the multiplier structure, a

typical scintillation pulse will yield 10^7 to 10^{10} electrons, sufficient to serve as a charge

signal for the original scintillation event. This charge is collected on the output stage of

the multiplier structure. More information of the characteristics and operating principles

of scintillators and photomultiplier tubes can be found elsewhere [7].
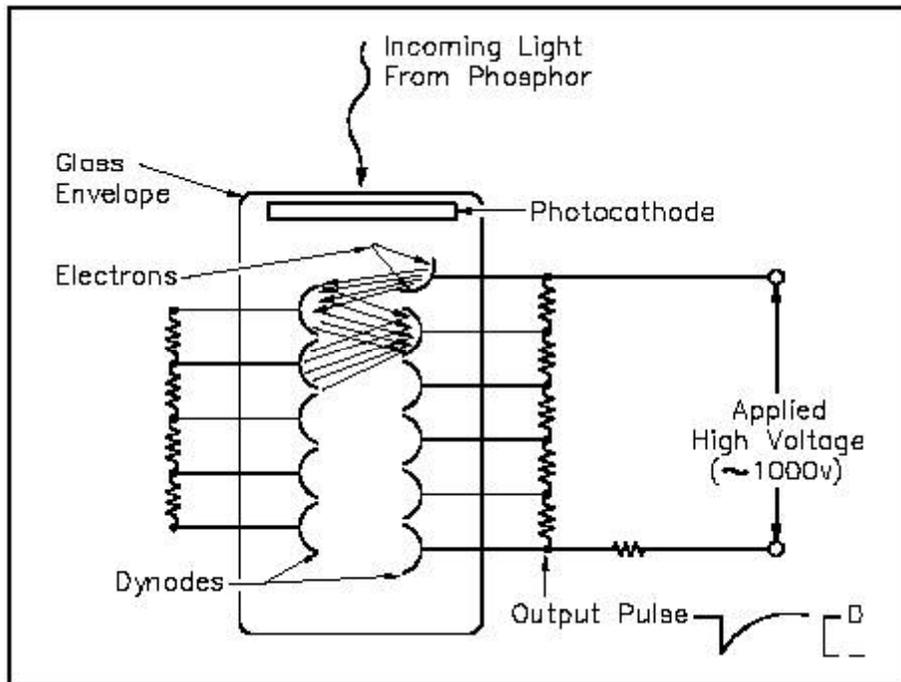
Figure 3.5. Scintillation photons incident on the photocathode are converted into
electrons by the photoelectric effect. The electrons are attracted to the nearest dynode and
several new electrons are generated. This amplification continues until the last dynode.

3.6   Electronics

The electronic pulses from the individual photomultiplier tubes are processed by various

electronic modules in order to select certain kinds of events and digitize the signals for

these events. Each photomultiplier tube is connected to an input on a discriminator

module. For each octant, there are four discriminator modules and each module contains

16 inputs. All four photomultiplier tubes of a given scintillator pair are connected to the

same discriminator. Thus, any discriminator module contains inputs for four scintillator

pairs. If an input signal from a photomultiplier tube exceeds the discriminator threshold

amplitude, then the discriminator module will output the signal to a coincidence unit and

a Time to Digital Converter (TDC) module. A TDC records the time difference between

a start and stop signal. The signal sent to the TDC goes to a "stop" channel. If the signal

sent to the Coincidence unit arrives when the computer is not busy, then the coincidence

unit will output the signal to a trigger supervisor. The trigger supervisor performs three

functions: it starts the TDC module, opens a gate in the Analog to Digital Converter

(ADC) module, and instructs the computer to look at data. The basic function of an ADC

is to produce a digital code at its output that is proportional to an analog voltage supplied

to its input. When the gate in the ADC module is opened, electric charge spills into it for

a specific width or time span (150 ns). The amount of charge accumulated in the gate is

integrated and stored on disk or tape. These data can be analyzed later to create an ADC

histogram. An ADC histogram displays the distribution of the photon energies seen by

the photomultiplier tubes. If a signal from a photomultiplier tube arrives before the gate

opens or after the gate closes, a good physics event will be lost.

3.7   Software

The data files are analyzed and processed using custom software (written using C++).

The G^0 Analysis package contains four executables: g0analysis, g0online, g0root, and

g0monitor. To analyze real data streams, g0online and g0monitor are used. To analyze

CODA files already on disc, g0analysis and g0root are used. For this thesis, the later

executables were used. G0analysis analyzes huge amounts of data retrieved off-line from

CODA files on disc. G0root is a ROOT-based [8] graphical framework customized for

the G^0 Experiment. It provides the means to make histograms and to perform fitting of ADC and TDC data from the scintillators.

4   Data Types

The data used in this thesis for testing the performance of the G^0 scintillators was of several kinds: cosmic ray, light emitting diode, and gain monitoring system, as described below.

4.1   Cosmic Ray Self-Trigger

The hardware-based cosmic ray self-trigger records a cosmic event when at least four photomultiplier tubes, located on the same discriminator, detect signals simultaneously. Cosmic rays are highly energetic particles, primarily protons, which cross interstellar space and enter the Earth's atmosphere. In the Earth's atmosphere, they interact with other particles and create cosmic showers of pions and muons. A pion is the lightest meson. A muon is a particle in the lepton family with a mass 207 times that of the electron and has other properties similar to those of the electron. Muons may have positive or negative electric charge. At sea level, about seventy-five percent of the surviving cosmic rays are muons. Cosmic muons are minimum ionizing particles (their energy loss per unit path length is small). Since the electrons that will be used in the G^0 experiment are minimum ionizing, cosmic muons make good test particles.

4.2   Light Emitting Diode

Each scintillator pair has two optical fibers, one attached at each end, which can be fed with the light from a common light emitting diode (LED). A LED is an easy way to test scintillator response to a known source of light. At a given time, the LED is connected to fibers at only one end of each of the 16 pairs of scintillators. The LED produces a

constant amount of visible light at a given location, at either the left or right end of the scintillator. The light is internally reflected until it reaches the ends of the scintillator and is transmitted via light guides to the photomultiplier tubes.

4.3   Gain Monitoring System

The gain monitoring system (GMS), a more sophisticated system than the LED, can be used to monitor changes in the detectors and photomultiplier tubes during data taking. The gain monitoring system is comprised of a nitrogen laser, optical fibers, and a rotating mask that enables illumination of a subset of fibers at a specified rate. The system flashes ultraviolet (UV) laser light directly into the scintillator via the same optical fibers as for the LED. This system is better than the LED system because high-frequency UV light will actually scintillate the plastic, just as the ionizing particles will. Problems with the nitrogen laser performance and stability have unfortunately prevented useful GMS data taking so far.

5   Octant 7 Analysis

5.1   LED Data Collection and Analysis

The purpose for these runs were to use LED and cosmic ray data to (a) verify that all channels of octant 7 were working, (b) to study the effects of the radiation environment on the performance of the detectors/photomultiplier tubes, and (c) to develop software to test the electronics and trigger. During LED data collection, only octant 7 was in the experimental hall (Hall C at Jefferson Lab). These data were taken before the octant was installed in the detector; instead it was on the floor of the hall. During some of this time, another experiment in the hall was running. This means that an electron beam was

present and contributed to significant background radiation in the hall. Both cosmic ray and LED triggers were enabled during some of these data-taking runs.

For each run analyzed, ADC histograms of both cosmic ray trigger events and LED events for all sixteen scintillator pairs in the octant were generated. Since events are recorded at both ends of a scintillator, histograms were produced for both the left and right photomultiplier tubes of each scintillator. Thus, for each scintillator pair in the octant, histograms were generated for the front right, front left, back right, and back left photomultiplier tubes. Each histogram was fitted to a Gaussian function and the mean amplitude and width of the function were computed as shown in Figure 5.1.

The Gaussian distribution describes the distribution of random observations for most experiments. It is accepted by convention and experimentation to be the most likely distribution. The Gaussian distribution function is defined as

$$P_{G(x,\mu,\sigma)} = \frac{1}{\sigma\sqrt{2\pi}} e^{\left[-\frac{1}{2}\left(\frac{x-\mu}{\sigma}\right)^2\right]}. \tag{4.1}$$

It is a continuous function describing the probability that from a parent distribution with a mean μ and a standard deviation σ, the value of a random observation would be x. The shape of a Gaussian function is a bell-shaped curve symmetric about the mean μ. The width of the curve is characterized by the full-width at half-maximum, which is called the half-width (FWHM $= 2.354\sigma$).

5.2   Absence of Cosmic Ray Events

Both the cosmic ray self-trigger event data and LED event data include the pedestal. A pedestal is the reading when no events have occurred in that ADC channel and is unique for each channel of the ADC. The pedestal readings determine the zero level of the electronics. A histogram of LED events for a run in which the LED is unplugged will include only the pedestal. These data were obtained deliberately as a way of measuring the individual pedestals. For runs of this type, a comparison of histograms of cosmic ray self-trigger events and LED events revealed that the two sets of histograms were identical. Figure 5.1 shows histograms of the back, right photomultiplier tube of scintillator 7 in Run 8389. The first histogram is of cosmic ray trigger events and the second histogram is of LED events. In this run, the LED was unplugged. Notice that the mean amplitudes of both event types are nearly the same. This indicates the absence of cosmic ray events and means that histograms of cosmic ray self-trigger events are a measure of the pedestal. This was unexpected and was a result of trigger mistiming (the analog pulse did not arrive at the ADC during the time that the ADC gate was on). This was corrected in later data taking (see Section 6). Thus, for the data taking with the single octant in the Hall, only the LED data were useful.
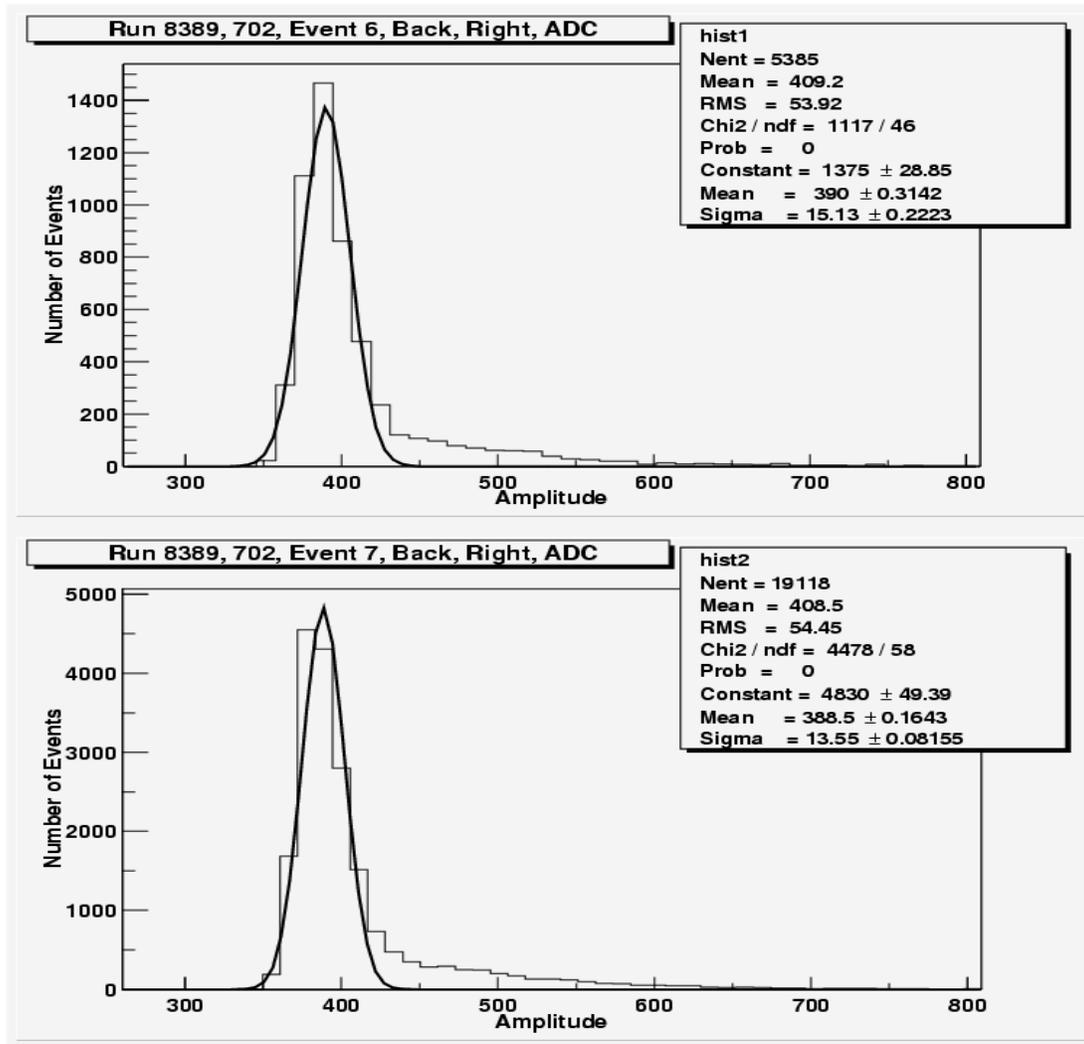
Figure 5.1. Histograms of the back, right photomultiplier tube of scintillator 7 in Run 8389. The upper histogram is of cosmic ray trigger events and the lower histogram is of LED events with the LED unplugged.

5.3   Histogram Tails

Scintillator pairs 1-8 show tails extending beyond the Gaussian function in histograms of

both the cosmic ray trigger events and LED events. Figure 5.2 shows tails in the

histograms of a typical case of the back, right photomultiplier tube on scintillator 3 in

Run 8390. During Run 8390, the beam was on. The first histogram shows cosmic ray

events and the second histogram displays LED events. A tail indicates that the scintillator

detected radioactivity from the room background. Collaborators at Jefferson lab have shown that the relative tail to pedestal ratio can be used as a measure of the background rate.

Room background includes low-energy gamma rays, X-rays, alpha particles, and low-energy electrons from beta decay of nuclei on the order of a few MeV or less. When there is beam in the experimental hall, neutrons are also produced and can contribute to the radioactivity in the room. When a neutron collides with a proton in a scintillator it recoils. Protons from neutron-induced reactions have a large dE/dx and thus produce light that can be detected.
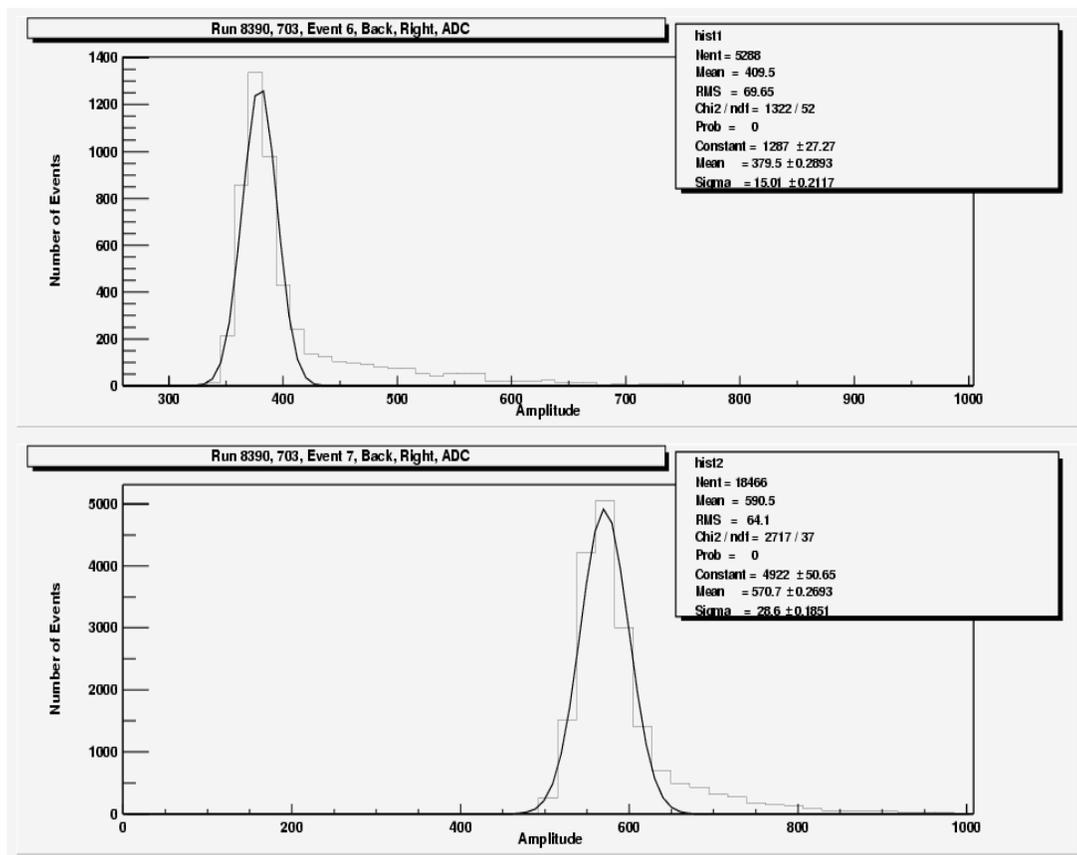
Figure 5.2. Histograms of the back, right photomultiplier tube on scintillator 3 in run 8390. The upper histogram is of cosmic ray trigger events and the lower histogram is of LED events.

In these data, scintillator pairs 9-16 do not have non-Gaussian tails extending beyond the Gaussian function. For example, Figure 5.3 includes two histograms of the back, right photomultiplier tube in Scintillator 14 in run 8390. The upper histogram is of cosmic ray trigger events and the lower histogram is of LED events. Notice that tails do not extend beyond the Gaussian functions. This indicates that the scintillators did not detect room background. The only possible explanation for this observation is that the high voltage on scintillator pairs 9-16 was turned off during this data taking. This was confirmed in the experiment log book.

5.4   Crosstalk

In these data, for scintillator pairs 1-8, the mean amplitude of LED events was observed to be greater than the mean amplitude of the pedestal. This observation is expected because voltage amplitudes of electronic noise are small compared to voltage amplitudes produced by the light from the LED. For scintillator pairs 9-16, the mean amplitude of the LED events was less than the mean amplitude of the pedestal for the runs investigated. Figure 5.3 shows histograms of cosmic ray trigger events and LED events for a run in which the mean amplitude of the pedestal was greater than the LED. Since the high voltage was turned off on scintillator pairs 9-16, LED signals were not generated. Thus, the mean amplitude of the pedestal and LED events should be the same. The negative mean amplitude of the LED events can be attributed to crosstalk between signal cables.
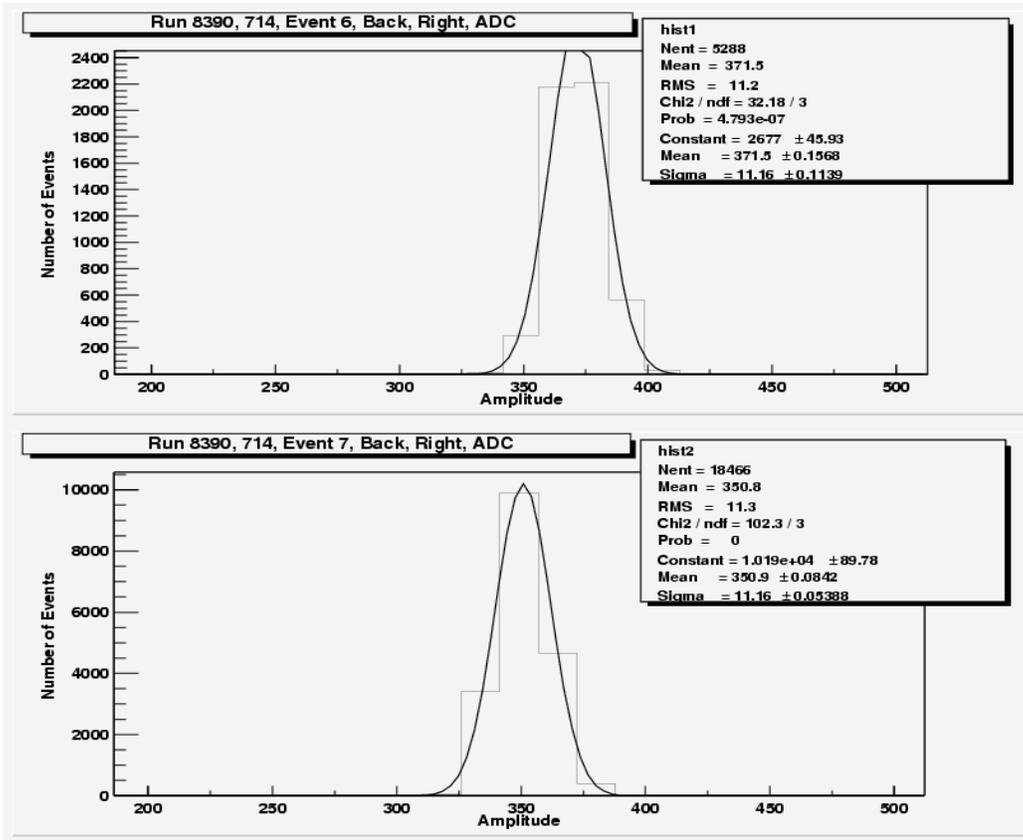
Figure 5.3. Histograms of the back, right photomultiplier tube of scintillator 14 in Run 8390. The upper histogram is of cosmic ray trigger events and the lower histogram is of LED events. The high voltage is turned off for this PMT.

Cables from scintillators that are physically adjacent, or from two tubes on the same scintillator, are kept far apart in the cable bundle. For example, a cable that connects a photomultiplier tube on Scintillator 1 to the ADC module runs alongside a cable that connects a photomultiplier tube of Scintillator 9 to the ADC module. Suppose a large signal is generated in Scintillator 1 and the high voltage is on. Since the cable connected to the photomultiplier tube on Scintillator 1 runs alongside the cable connected to the photomultiplier tube on Scintillator 9, the cable connected to Scintillator 9 experiences a small and opposite polarity induced voltage. In other words, Scintillator 9 shows an apparent decrease in the mean amplitude of LED events. Thus, the pedestal

appears to be larger than the amplitude of the LED events. So, if there is a real pulse generated in Scintillator 9, its apparent amplitude (ADC value) would be reduced due to this crosstalk. For example, consider the histogram of the back, right photomultiplier tube of scintillator 14 in Run 8390 (Figure 5.3). The effect of crosstalk on the amplitude of this photomultiplier tube is 14%. This effect is significant and presents a serious problem.

The gain monitoring system will provide a means by which to measure the crosstalk. For example, suppose the rotating mask is set to illuminate a specific photomultiplier tube. By measuring the amplitudes of the other 63 photomultiplier tubes in the octant and subtracting from them their corresponding pedestals, one can determine the crosstalk.

5.5   Detector Degradation

Because the G^0 detector will be exposed to sustained high levels of radiation, considerable attention must be given to the effects of the radiation environment on the performance of the photomultiplier tubes. To analyze these effects, two plots were generated of the mean LED amplitude versus time for a subset of photomultiplier tubes in a given set of runs. Pedestals were subtracted from the mean LED amplitude. The first plot includes times up to 5.5 days. The second plot includes times between 5.5 and 11 days. For times up to 5.5 days, most of the photomultiplier tubes show an upward trend in mean LED amplitude as shown in Figure 5.4. The increases in mean LED amplitudes of the photomultiplier tubes range from 0.5-2 % of the original amplitudes at time zero. This indicates a tendency toward recovery or annealing of the damage over periods of time that may be hours or days following an exposure. This trend is not understood.
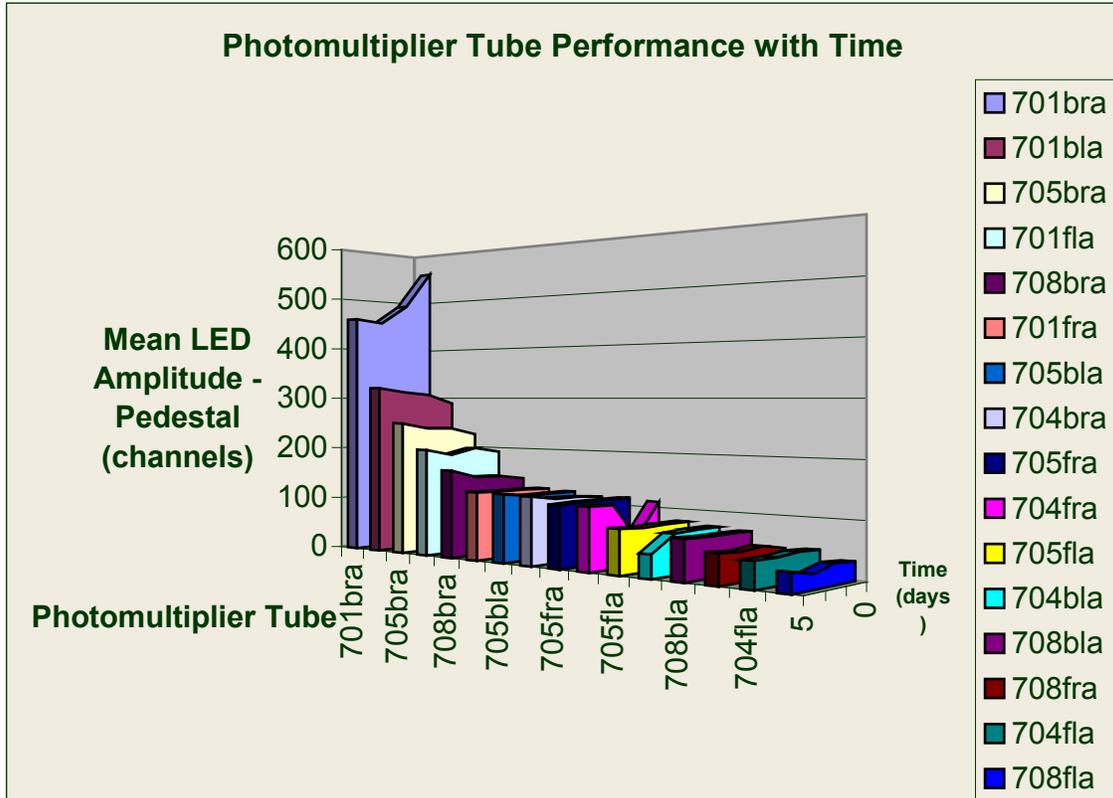
Figure 5.4. Photomultiplier tube performance with time of octant 7 up to 5.5 days. Data includes runs 8328, 8340, 8345, 8373, and 8390. Each color corresponds to a different photomultiplier tube. In the legend, the first number indicates the scintillator number (1-8), the second and third numbers indicate the scintillator number (01-16), the first two letters indicate the photomultiplier tube (front left, front right, back left, back right), and the last letter indicates ADC.

For times between 5.5 and 11 days, many of the photomultiplier tubes showed a downward trend as shown in Figure 5.5. The decrease in mean LED amplitudes range from 0.5-2% of the amplitude at 5.5 days. This effect is most likely caused by the aging of the photomultiplier tubes due to the high current drawn from them. Degradation of photomultiplier tubes with time presents a serious problem to the G^0 experiment since the measurement requires several months of beam. To preserve the photomultiplier tubes, the high voltage will be reduced and electronic amplifiers will be added.
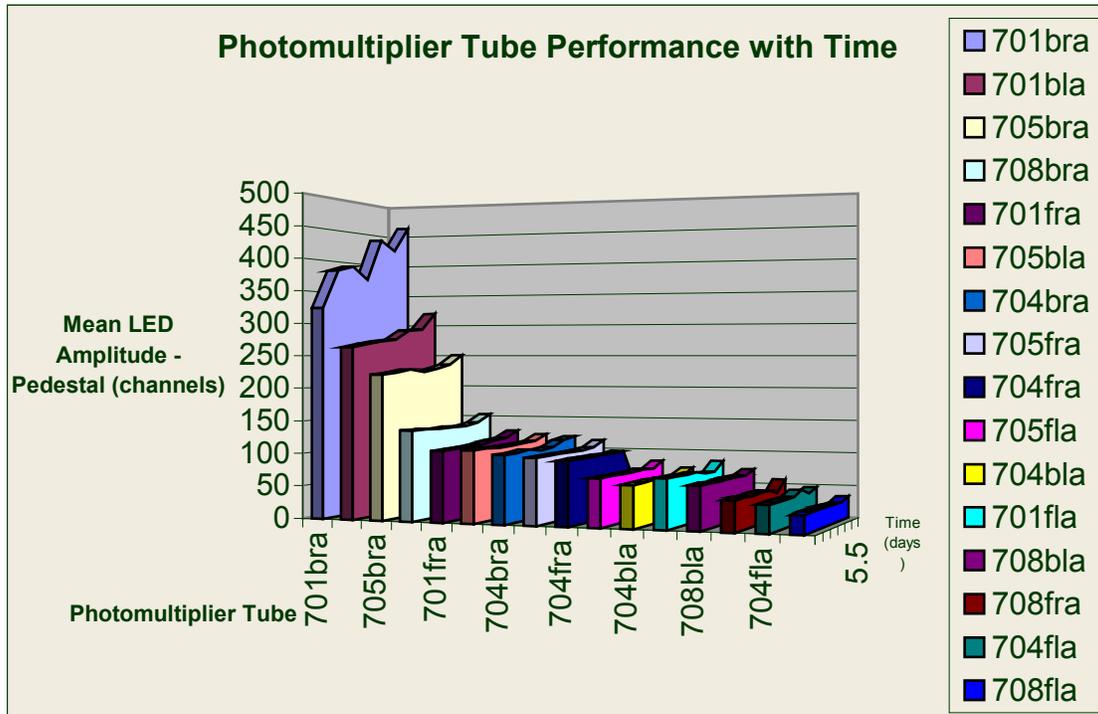
Figure 5.5. Photomultiplier tube performance with time of octant 7 for days 5.5 to 12. Data includes runs 8394, 8398, 8401, 8416, 8421, 8428. Each line corresponds to a different photomultiplier tube. In the legend, the first number indicates the scintillator number (1-8), the second and third numbers indicate the scintillator number (01-16), the first two letters indicate the photomultiplier tube (front left, front right, back left, back right), and the last letter indicates ADC.

6   Cosmic Ray Analysis and Interpretation of Results

6.1   Cosmic Data Collection and Analysis

The purpose for these runs are to use cosmic ray induced data to (a) verify that all

channels of the North American octants are working, (b) assess the performance of the

hardware-based cosmic ray trigger, and (c) develop the techniques to allow cosmic rays

to be used as a periodic check on detector performance. During cosmic data collection, all

four of the North American octants (numbered 1,3,5 and 7) were installed in the detector.

Figure 6.1 shows the location and numbering of the eight octants in the detector.
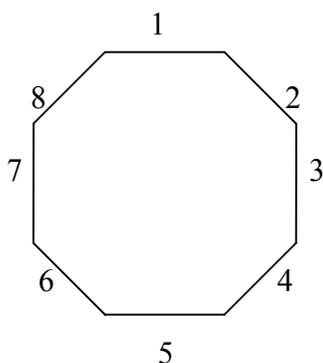
Figure 6.1. Location and numbering of the eight octants in the detector with the beam directed into the page. Octants 1,3,5, and 7 are North American octants.

For each run analyzed, ADC histograms of cosmic ray events for a subset of scintillator pairs in the four North American octants were generated. Each histogram was fitted to a Landau function and the most probable amplitude and sigma of the function were computed as shown in Figure 6.3. The Landau distribution describes the fluctuations of energy loss by ionization of a charged particle in a thin layer of matter. The fluctuations give rise to an asymmetric probability density function which is characterized by a narrow peak and a long tail towards positive values. The tail is due to the small number of collisions with a small probability of transferring large amounts of energy.

6.2   Software Triggers

The hardware-based cosmic ray self-trigger records a cosmic event when at least two pairs of photomultiplier tubes, located on different scintillators, detect signals simultaneously. To assess the performance of the hardware-based cosmic ray trigger, several different software-based triggers were created in G0Root macros: "1-hit", "4-hits", and "5-hits" (see Appendix B). The "1-hit" software-based trigger records a cosmic

ray event in a given photomultiplier tube when the TDC has fired on that photomultipler tube. This criteria allows hits above the discriminator threshold that were detected in that photomultiplier tube to count as a cosmic ray event when three other photomultiplier tubes (out of a group of 16) get a hit. These three other hits may originate from a cosmic ray or may be low energy noise that hit simultaneously.

The "4-hits" software-based trigger records a cosmic ray event for a given photomultiplier tube in a scintillator pair when the TDC is fired on all four photomultiplier tubes that view the two scintillators in that pair. This criteria eliminates many of the low energy hits detected by the "1-hit" software-based trigger because it localizes a small region of the octant. It is less probable that low energy particles will hit all four photomultiplier tubes of the given scintillator pair simultaneously. The "5-hits" software-based trigger records a cosmic ray event in a given part of a scintillator when the TDC is fired on all four photomultiplier tubes of the given scintillator pair and the back, right part of the scintillator located adjacent and behind (layer +1) the given scintillator. This criteria eliminates much of the low energy hits detected by the "4-hits" trigger because it further selects for events that go through a pair of scintillators (and are therefore more likely to be high-energy cosmic rays). It is less probable that low energy particles will simultaneously hit all four photomultiplier tubes of the given scintillator pair as well as one part of the scintillator located adjacent to the given scintillator. Figure 6.2 shows a superposition of ADC histograms for the three software-based triggers.
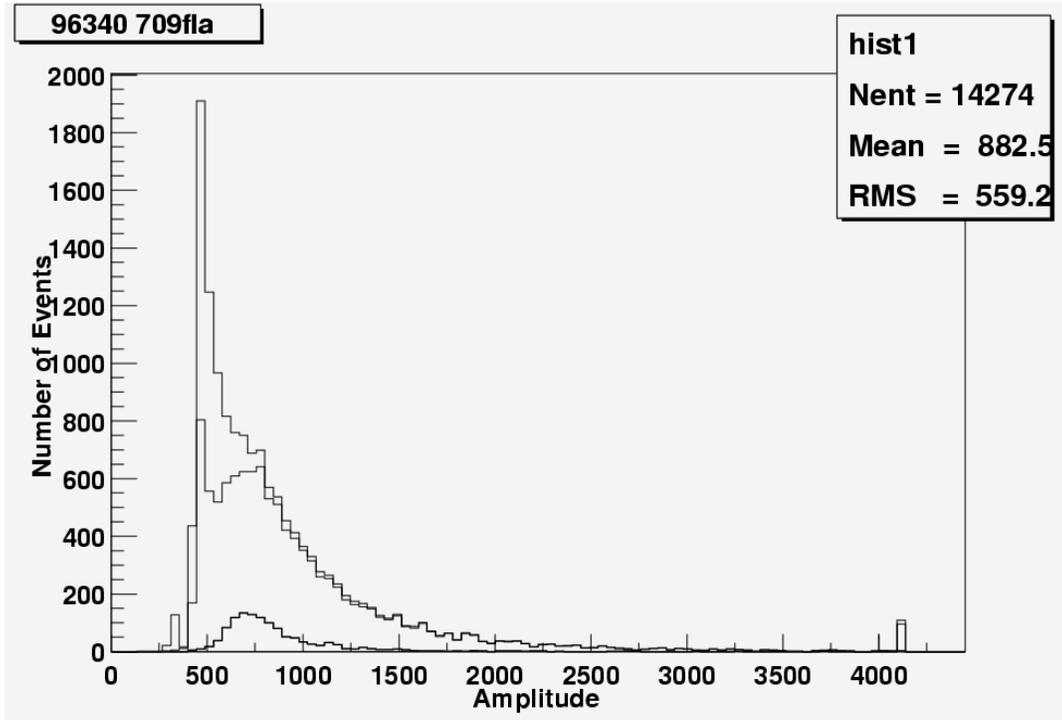
Figure 6.2. A superposition of ADC histograms for the three software-based triggers of the front, left photomultiplier tube on Scintillator 9 in Octant 7 in Run 96340. The histogram with the largest peak is the "1-hit" trigger, the histogram with the middle peak is the "4-hits" trigger, and the histogram with the smallest peak is the "5-hits" trigger.

The histogram of the "1-hit" trigger is a falling exponential cut off by the discriminator threshold at approximately 400 units. The histogram of the "4-hits" trigger has a peak at approximately 700 units on a smooth background. Similarly, the histogram of the "5-hits" trigger has a peak at approximately 750 units on a smooth background. The ascent becomes more gradual due to the elimination of low energy amplitudes.

6.3   Unbiased Trigger

To further assess the performance of the hardware-based cosmic ray trigger, a fourth

software-based trigger was created and called the "unbiased" trigger. This trigger records

a cosmic ray event in a given photomultiplier tube when the TDC is fired in all four

photomultiplier tubes of each scintillator located on either side (layer − 1 and layer + 1)

of the given scintillator. This criterion selects particles with a particular trajectory by

requiring that the particle traverse two scintillators, located one scintillator apart. Figure

6.3 shows an ADC histogram of the "unbiased" cosmic ray trigger.
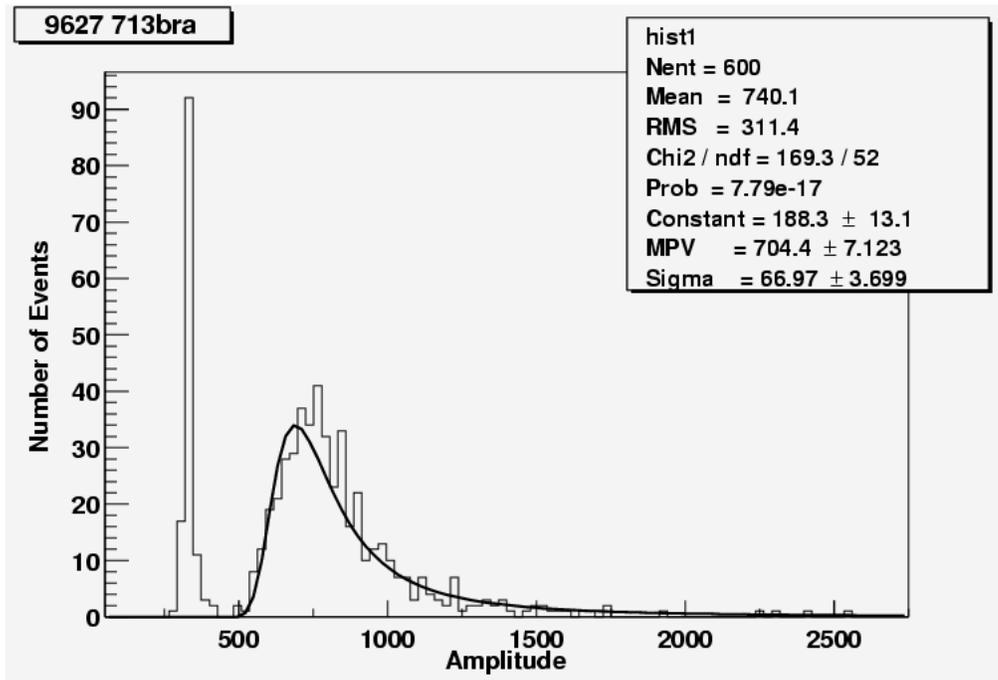
Figure 6.3. ADC histogram of an "unbiased" cosmic ray trigger of the back, right
photomultiplier tube on Scintillator 13 in Octant 9 in Run 9627.

The Landau distribution of the photon energies of an "unbiased" cosmic ray trigger is similar to that of a "5-hits" cosmic ray trigger. The peak is narrow and the tail is long. In contrast, the histogram of an "unbiased" cosmic ray trigger includes the pedestal whereas the histogram of a "5-hits" cosmic ray trigger does not. This is because the "unbiased" cosmic ray trigger does not require that the TDC for that given photomultiplier tube fire. Thus its pulse height can be below the discriminator threshold. Another important difference is that the amplitude distribution of the "unbiased" cosmic ray trigger is narrower than the amplitude distribution of the "5-hits" cosmic ray trigger. This is a result of the fact that the "unbiased" cosmic ray trigger requires a better defined geometry. The "unbiased" trigger requires that the particle pass through two scintillators, located one scintillator apart. The "5-hits" trigger requires that the particle traverses 2 scintillators adjacent to each other. This difference is illustrated in Figure 6.4.
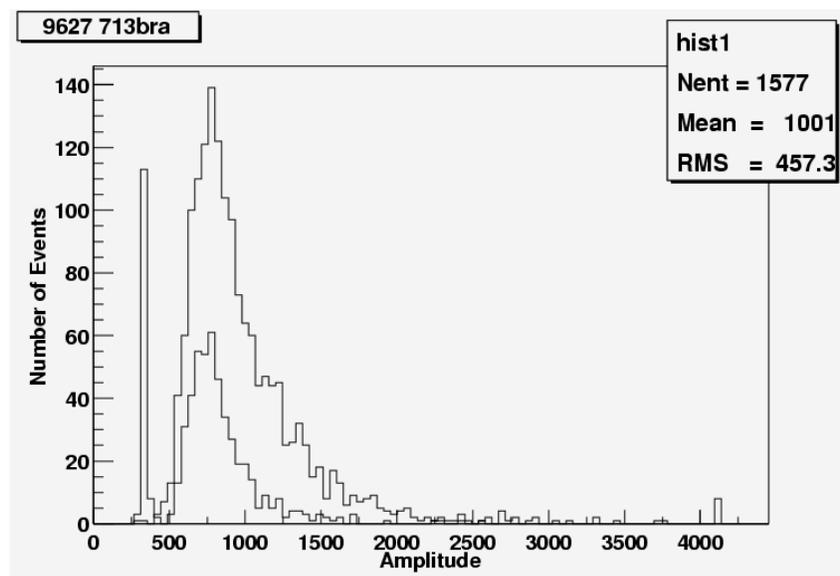
Figure 6.4. A superposition of ADC histograms of the "unbiased" and "5-hits" cosmic ray triggers of the back, right photomultiplier tube on scintillator 13 in octant 7 in run 9627. The histogram with the largest peak is the "5-hits" trigger, and the histogram with the smallest peak is the "unbiased" trigger. The pedestal, located at about 400 channels, corresponds to the "unbiased" trigger.

6.4   Run-to-Run Variation

To evaluate the variation in the most probable amplitudes of the scintillators from run to run, a plot was generated (Figure 6.5) of the average ADC most probable value versus scintillator number (averaging over the 4 photomultiplier tubes: front right, front left, back right, back left) for the third octant using the software-based "5-hits" cosmic ray trigger. Different geometrical shapes and colors represent different runs. An overlapping of shapes indicates consistency in the most probable amplitude for a given scintillator among different runs, whereas a vertical spread between shapes represents a variation in the most probable amplitude for a given scintillator among different runs.
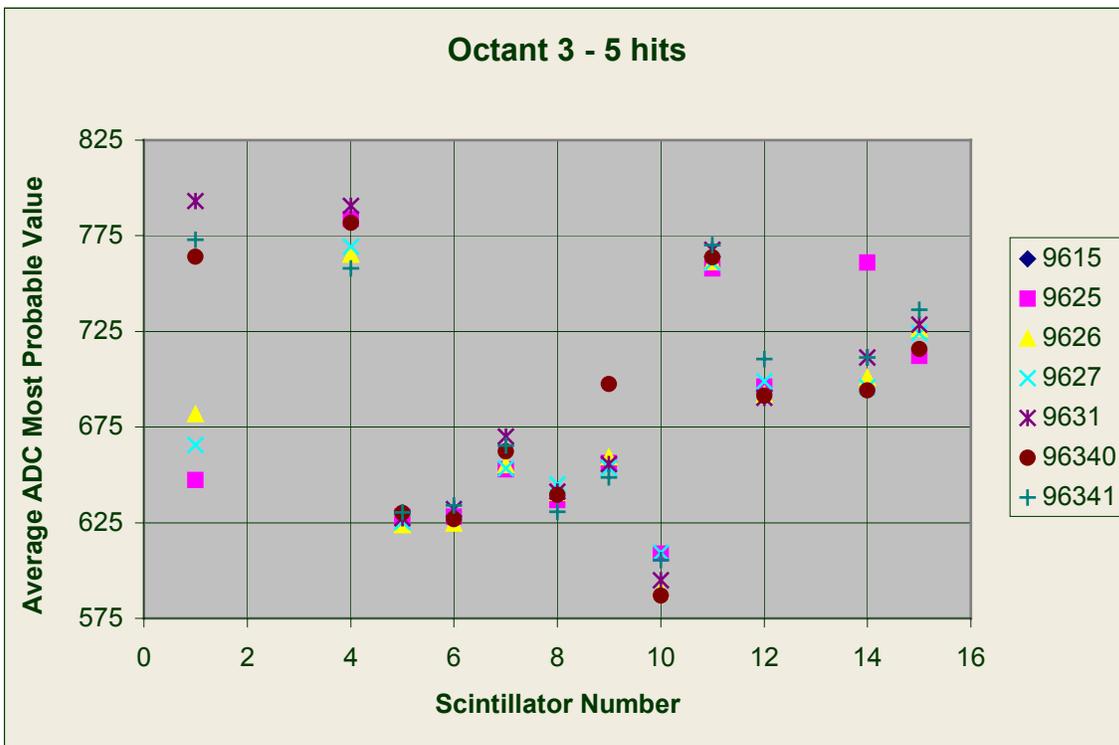
Figure 6.5. Average ADC most probable value versus scintillator number for Octant 3 using the software-based "5-hits" cosmic ray trigger. Different geometrical shapes and colors represent different runs. Pedestals were not subtracted. Scintillators 2,3,13, and 16 are not included because they were not working correctly.

With a few exceptions, the standard deviations or the spread in the most probable

amplitudes for scintillators in octant 3, using the "5-hits" software-based cosmic ray

trigger, range from 2-12%. The standard deviations are comparable with errors on the

most probable value from fits to Landau functions for typical runs. The standard

deviations are given in Table 6.1.

Table 6.1. Standard deviations in the most probable amplitude of scintillators in Octant 3.

Scintillator Number	Standard Deviation (%)	Scintillator Number	Standard Deviation (%)
1	56	9	16
4	11	10	11
5	2	11	8
6	4	12	12
7	6	14	24
8	5	15	8

The small standard deviations suggest that the photomultiplier tubes are stable with time.

Since the beam is off, the numbers imply that there is no large background to degrade the

performance of the photomultiplier tubes. Variations from layer to layer are not

understood.

6.5   High Voltages

To assess the high voltage on each photomultiplier tube, a plot was generated (Figure 6.6)

of the ADC most probable amplitude versus photomultiplier tube for octant 3 using the

software-based "5-hits" cosmic ray trigger. Along the x-axis, there are 64 channels that

can be divided into 16 groups of 4. These groups of four represent the front right, front

left, back right, and back left photomultiplier tubes of a given scintillator pair. The

scintillator number increases along the positive x-direction.
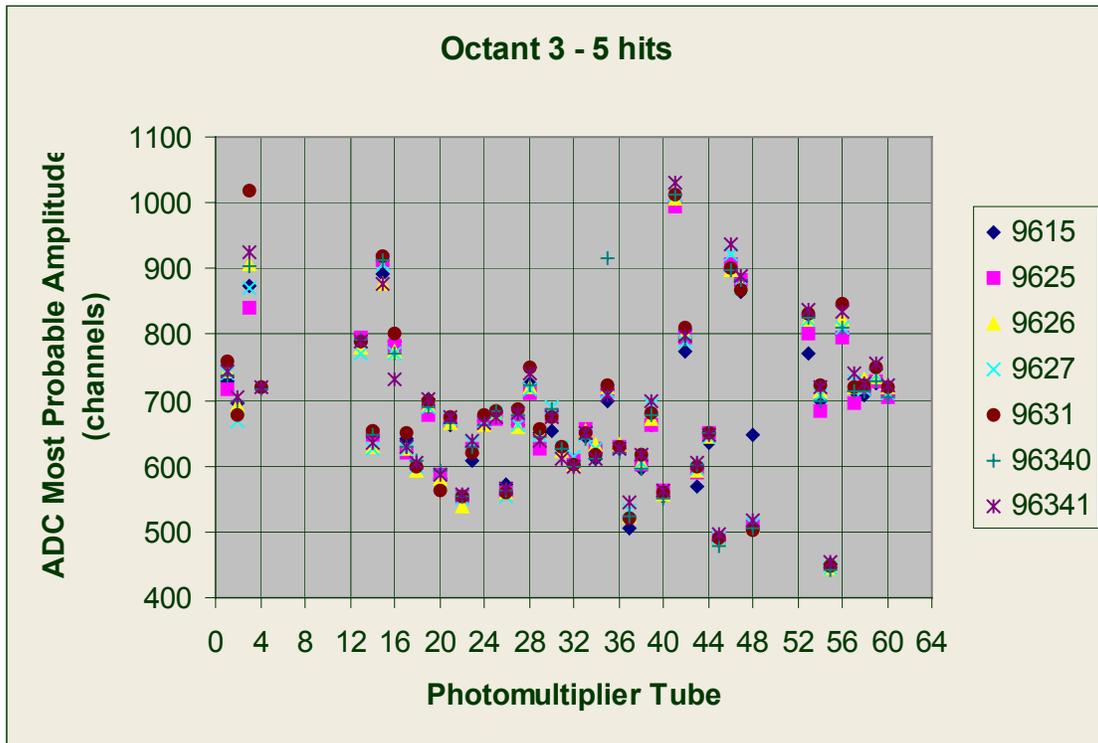
Figure 6.6. ADC most probable values amplitudes versus photomultiplier tube for octant 3 using the software-based "5-hits" cosmic ray trigger. Scintillators 2,3,13, and 16 are not included because they were not working correctly.

To provide uniform response to minimum ionizing particles, adjustments are necessary to balance the high voltages of the photomultiplier tubes. For example, consider the most probable amplitudes of the front right, front left, back right, and back left photomultiplier tubes on Scintillator 4 (units 13-16 on the x-axis). Compared to the first and fourth marks, the second mark is significantly smaller in amplitude, and the third mark is significantly larger in amplitude. To balance the high voltages on Scintillator 4, the high voltage of the front left photomultiplier tube must raised, and the high voltage on the back right photomultiplier tube must be lowered.

6.6   Trends in ADC Most Probable Amplitude Versus Scintillator Number

To look for trends in the ADC most probable amplitude versus scintillator number, a plot

was generated (Figure 6.7) of ADC most probable values versus scintillator for octant 3.

Plotted along the x-axis are 448 channels that can be divided into seven groups of 64

channels. Each group of 64 channels represents a run that can be divided further into 16

groups of 4. Each group of 4 represents the front left, front right, back left, and back right

photomultiplier tubes on a scintillator. Scintillator number and run number increase along

the positive x-direction. Different geometrical shapes and colors represent different

software-based cosmic ray triggers.
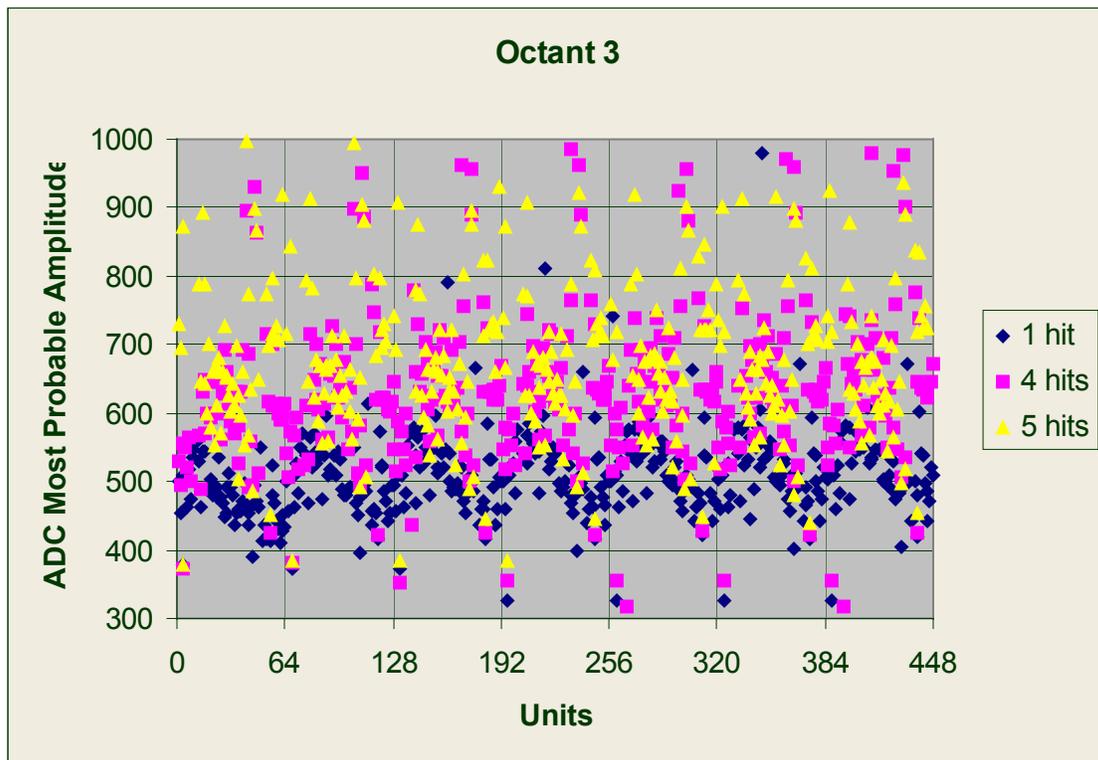
Figure 6.7. ADC most probable amplitude versus photomultiplier tube of Octant 3 for
seven runs using different software-based cosmic ray triggers.

For the "1-hit" software-based cosmic ray trigger, there is a periodic 'zig zag' of the most probable amplitude with run number. For the "5-hits" software-based cosmic ray trigger, there is a periodic trend that is out of phase with the 'zig zag' of the "1-hit" software based cosmic ray trigger. The minimum of the "1-hit" coincides with the maximum of the "5-hits" and vice versa. For the "4-hits" software based trigger, a pattern is difficult to distinguish. At this time, the trends cannot be explained.

7   Conclusions

To evaluate the performance of the detectors, studies were performed on analog to digital converter data of both light emitting diode events and cosmic ray events. Studies of light emitting diode events included data from Octant 7 when it was on the floor of the hall. From these studies, several results were extracted. First, a cosmic ray trigger timing problem was detected by the absence of cosmic ray events from the data. The analog pulse did not arrive at the ADC during the time that the ADC gate was open. This was corrected by our collaborators for later data-taking. Second, histogram tails can be used as background diagnostics. Tails indicate that room background was detected such as X-rays and alpha particles. When the high voltage to the photomultiplier tubes is turned on, tails will extend beyond the Gaussian function. When the high voltage is turned off, tails will not extend beyond the Gaussian function. Third, crosstalk can be detected by a comparison of the mean amplitude of the pedestal and the mean amplitude of LED events when the high voltage is off. When the high voltage is turned off, LED signals are not generated. Thus, the mean amplitudes of the pedestal and LED events should be the same. Under these conditions, crosstalk exists when the mean amplitude of the LED is less than the

mean amplitude of the pedestal. Fourth, photomultiplier tube degradation with time was found to be a serious problem. Over a period of days, the mean LED amplitude for a subset of photomultipler tubes in a given set of runs decreased between 0.5-2%. To preserve the photomultiplier tubes, the high voltage will be reduced and amplifiers will be added.

Analyses of cosmic ray events included data from all four of the North American octants. During data collection, all of the octants were installed in the detector. From these analyses, many conclusions were made. First, the hardware-based cosmic ray trigger was found to be rather unselective. Multiple software-based cosmic ray triggers were created in G^0 macros and their ADC histograms were compared with histograms of the hardware-based cosmic ray trigger. The hardware-based trigger did not differentiate cosmic rays well from low energy noise. The "5-hits" and "unbiased" software-based cosmic ray triggers eliminate much of the low energy hits because they localize a small region of the octant and requires a physically meaningful coincidence. Second, the standard deviation in the most probable amplitude of any scintillator, from run to run, ranges from 2-12%. Third, to provide uniform response to minimum ionizing particles, adjustments to the high voltages on the photomultiplier tubes are necessary. Fourth, trends in the ADC most probable amplitude versus scintillator number exist but cannot be explained. Cosmics can be used as a diagnostic, but more investigation is needed to understand the trends.

There are several lines of work arising from this thesis that will be pursued in the future. First, following from Sections 5.5 and 6.5, high voltages on the photomultiplier tubes will be adjusted by collecting and analyzing more cosmic ray

data after amplifiers are installed. A second line of work, which follows from Section 6.6, is to perform more data analysis to understand trends in the ADC most probable amplitude versus scintillator number. Third, following from Section 5.4, crosstalk will be examined by using the gain monitoring system. Finally, the gain monitoring system will be cross-calibrated with cosmic ray data.

Currently, the magnet is being installed in the hall. The target is scheduled for installation during the summer. The first tests with the beam will begin in late August and the first run will be this fall.

Appendix

A   ADC Cosmic and LED Event Macro

The following macro is user-interactive and generates ADC histograms for a given run number and photomultiplier tube of both the cosmic self-trigger and LED event data. It generates histograms for the back left, back right, front left, and front right. It fits the histograms to a gaussian and calculates the mean and width of the gaussian. Results of the fits are stored in an ASCII text file for further analysis.

```
{
ofstream DataFile;
DataFile.open("dmeannwidth.txt",ios::app);

TString octant="7";
TString scint;
TString run;
TString histogram;
TString event;

cout<<"Enter run number: ";
cin>>run;
cout<<"Enter scintillator number (01-16): ";
cin>>scint;

// to have the parameters of the fit displayed
gStyle->SetOptFit(1111);

TAnalysis ana("SetupChainTest.05-25-01.dat");
//gROOT->SetStyle("plain");

ana.SetROOTFileName("G0Scaler."+run+".root");

TCanvas c1;
c1.Divide(2,4);

//Generates a histogram of back, right, ADC, cosmic self-trigger
c1.cd(1);
ana.Plot(octant+scint+"bra>>hist1","evt_type==6");
hist1.Fit("gaus");
hist1->GetXaxis()->SetTitle("Amplitude");
hist1->GetXaxis()->CenterTitle();
hist1->GetYaxis()->SetTitle("Number of Events");
hist1->GetYaxis()->CenterTitle();
hist1->SetTitle("Run "+run+", "+octant+scint+", Event 6, Back, Right, ADC");
TF1 *fit1=hist1->GetFunction("gaus");
mean =fit1->GetParameter(1);
emean=fit1->GetParError(1);
sigma =fit1->GetParameter(2);
esigma=fit1->GetParError(2);
histogram=octant+scint+"bra";
event="6";
DataFile<<"run  histogram  event    mean       emean      sigma     esigma \n";
DataFile<<run<<" "<<histogram<<"      "<<event<<"         ";
DataFile<<mean<<"      "<<emean<<"     "<<sigma<<"     "<<esigma<<"\n";

//Generates a histogram of back, right, ADC, LED event
c1.cd(2);
```

```
ana.Plot(octant+scint+"bra>>hist2","evt_type==7");
hist2.Fit("gaus");
hist2->GetXaxis()->SetTitle("Amplitude");
hist2->GetXaxis()->CenterTitle();
hist2->GetYaxis()->SetTitle("Number of Events");
hist2->GetYaxis()->CenterTitle();
hist2->SetTitle("Run "+run+", "+octant+scint+", Event 7, Back, Right, ADC");
TF1 *fit2=hist2->GetFunction("gaus");
mean =fit2->GetParameter(1);
emean=fit2->GetParError(1);
sigma =fit2->GetParameter(2);
esigma=fit2->GetParError(2);
histogram=octant+scint+"bra";
event="7";
DataFile<<run<<" "<<histogram<<"      "<<event<<"          ";
DataFile<<mean<<"    "<<emean<<"   "<<sigma<<"   "<<esigma<<"\n";

//Generates a histogram of back, left, ADC, cosmic self-trigger
c1.cd(3);
ana.Plot(octant+scint+"bla>>hist3","evt_type==6");
hist3.Fit("gaus");
hist3->GetXaxis()->SetTitle("Amplitude");
hist3->GetXaxis()->CenterTitle();
hist3->GetYaxis()->SetTitle("Number of Events");
hist3->GetYaxis()->CenterTitle();
hist3->SetTitle("Run "+run+", "+octant+scint+", Event 6, Back, Left, ADC");
TF1 *fit3=hist3->GetFunction("gaus");
mean =fit3->GetParameter(1);
emean=fit3->GetParError(1);
sigma =fit3->GetParameter(2);
esigma=fit3->GetParError(2);
histogram=octant+scint+"bla";
event="6";
DataFile<<run<<" "<<histogram<<"      "<<event<<"          ";
DataFile<<mean<<"    "<<emean<<"   "<<sigma<<"   "<<esigma<<"\n";

//Generates a histogram of back, left, ADC, LED event
c1.cd(4);
ana.Plot(octant+scint+"bla>>hist4","evt_type==7");
hist4.Fit("gaus");
hist4->GetXaxis()->SetTitle("Amplitude");
hist4->GetXaxis()->CenterTitle();
hist4->GetYaxis()->SetTitle("Number of Events");
hist4->GetYaxis()->CenterTitle();
hist4->SetTitle("Run "+run+", "+octant+scint+", Event 7, Back, Left, ADC");
TF1 *fit4=hist4->GetFunction("gaus");
mean =fit4->GetParameter(1);
emean=fit4->GetParError(1);
sigma =fit4->GetParameter(2);
esigma=fit4->GetParError(2);
histogram=octant+scint+"bla";
event="7";
DataFile<<run<<" "<<histogram<<"      "<<event<<"          ";
DataFile<<mean<<"    "<<emean<<"   "<<sigma<<"   "<<esigma<<"\n";

//Generates a histogram of front, right, ADC, cosmic self-trigger
c1.cd(5);
ana.Plot(octant+scint+"fra>>hist5","evt_type==6");
hist5.Fit("gaus");
hist5->GetXaxis()->SetTitle("Amplitude");
hist5->GetXaxis()->CenterTitle();
hist5->GetYaxis()->SetTitle("Number of Events");
hist5->GetYaxis()->CenterTitle();
```

```
hist5->SetTitle("Run "+run+", "+octant+scint+", Event 6, Front, Right, ADC");
TF1 *fit5=hist5->GetFunction("gaus");
mean =fit5->GetParameter(1);
emean=fit5->GetParError(1);
sigma =fit5->GetParameter(2);
esigma=fit5->GetParError(2);
histogram=octant+scint+"fra";
event="6";
DataFile<<run<<" "<<histogram<<"      "<<event<<"         ";
DataFile<<mean<<"     "<<emean<<"    "<<sigma<<"    "<<esigma<<"\n";

//Generates a histogram of front, right, ADC, LED event
c1.cd(6);
ana.Plot(octant+scint+"fra>>hist6","evt_type==7");
hist6.Fit("gaus");
hist6->GetXaxis()->SetTitle("Amplitude");
hist6->GetXaxis()->CenterTitle();
hist6->GetYaxis()->SetTitle("Number of Events");
hist6->GetYaxis()->CenterTitle();
hist6->SetTitle("Run "+run+", "+octant+scint+", Event 7, Front, Right, ADC");
TF1 *fit6=hist6->GetFunction("gaus");
mean =fit6->GetParameter(1);
emean=fit6->GetParError(1);
sigma =fit6->GetParameter(2);
esigma=fit6->GetParError(2);
histogram=octant+scint+"fra";
event="7";
DataFile<<run<<" "<<histogram<<"      "<<event<<"         ";
DataFile<<mean<<"     "<<emean<<"    "<<sigma<<"    "<<esigma<<"\n";

//Generates a histogram of front, left, ADC, cosmic-self trigger
c1.cd(7);
ana.Plot(octant+scint+"fla>>hist7","evt_type==6");
hist7.Fit("gaus");
hist7->GetXaxis()->SetTitle("Amplitude");
hist7->GetXaxis()->CenterTitle();
hist7->GetYaxis()->SetTitle("Number of Events");
hist7->GetYaxis()->CenterTitle();
hist7->SetTitle("Run "+run+", "+octant+scint+", Event 6, Front, Left, ADC");
TF1 *fit7=hist7->GetFunction("gaus");
mean =fit7->GetParameter(1);
emean=fit7->GetParError(1);
sigma =fit7->GetParameter(2);
esigma=fit7->GetParError(2);
histogram=octant+scint+"fla";
event="6";
DataFile<<run<<" "<<histogram<<"      "<<event<<"         ";
DataFile<<mean<<"     "<<emean<<"    "<<sigma<<"    "<<esigma<<"\n";

//Generates a histogram of front, left, ADC, LED event
c1.cd(8);
ana.Plot(octant+scint+"fla>>hist8","evt_type==7");
hist8.Fit("gaus");
hist8->GetXaxis()->SetTitle("Amplitude");
hist8->GetXaxis()->CenterTitle();
hist8->GetYaxis()->SetTitle("Number of Events");
hist8->GetYaxis()->CenterTitle();
hist8->SetTitle("Run "+run+", "+octant+scint+", Event 7, Front, Left, ADC");
TF1 *fit8=hist8->GetFunction("gaus");
mean =fit8->GetParameter(1);
emean=fit8->GetParError(1);
sigma =fit8->GetParameter(2);
esigma=fit8->GetParError(2);
```

```
histogram=octant+scint+"fla";
event="7";
DataFile<<run<<" "<<histogram<<"      "<<event<<"         ";
DataFile<<mean<<"    "<<emean<<"   "<<sigma<<"   "<<esigma<<"\n";

DataFile.close();

}
```

B   ADC Cosmic Ray Software-Based Trigger for 5-Hits Macro

The following macro is user-interactive and generates ADC histograms for a given run number of the cosmic self-trigger event data. It requires that the TDC on all four parts of a given scintillator (front right, front left, back right, back left) fire as well and the TDC on the back right part of the scintillator above the given scintillator. It generates histograms for the back left, back right, front left, and front right parts of every scintillator in every installed octant. It fits the histograms to a landau and calculates the most probable value of the landau. Results of the fits are stored in an ASCII text file and histograms are saved in a postscript file for further analysis. This macro can be modified to require different numbers and types of cuts.

```
{

// to have the parameters of the fit displayed
gStyle->SetOptFit(1111);
TAnalysis ana("Setup.11-07-01.dat");

ofstream DataFile;
DataFile.open("cosmics5hits.txt",ios::app);
DataFile<<"run     hist       mean          emean        sigma
esigma \n";

int scintnum=1;
int octantnum;
int n=1;
TString run;
TString octant;
TString scint;
TString histogram;
TString scintplus;

cout<<"Enter run number: ";
cin>>run;

ana.SetROOTFileName("/scratch/armd/work/G0Scaler."+run+".root");

TPostScript *ps = new TPostScript("Cosmic"+run+".ps",112);

ps->NewPage();
TCanvas c1;
c1.Divide(2,2);

ana.SetLoopPattern("hist%","1:64:1");
ana.ShowLoop();    //This just writes things to the screen, so I see
that I have created the correct strings

//Increment octants by 2 because North American octants are odd
numbers.
for (octantnum=3; octantnum<8; octantnum=octantnum+4)
  {

  if (octantnum==1)
      octant="1";
```

```
if (octantnum==3)
    octant="3";
if (octantnum==5)
    octant="5";
if (octantnum==7)
    octant="7";

while (scintnum<17)
  {

     // n controls plot number and when to update the canvas and
     //go to a new page.

     while (n<4 )
      {

      if (scintnum==1)
      {
      scint="01";
      scintplus="02";
      }
      if (scintnum==2)
      {
      scint="02";
        scintplus="03";
      }
      if (scintnum==3)
      {
      scint="03";
      scintplus="04";
      }
      if (scintnum==4)
      {
      scint="04";
        scintplus="05";
      }
      if (scintnum==5)
      {
      scint="05";
      scintplus="06";
      }
      if (scintnum==6)
      {
      scint="06";
      scintplus="07";
      }
      if (scintnum==7)
      {
      scint="07";
      scintplus="08";
      }
      if (scintnum==8)
      {
      scint="08";
      scintplus="09";
      }
      if (scintnum==9)
```

```
        {
        scint="09";
        scintplus="10";
        }
        if (scintnum==10)
        {
        scint="10";
        scintplus="11";
        }
        if (scintnum==11)
        {
        scint="11";
        scintplus="12";
        }
        if (scintnum==12)
         {
         scint="12";
         scintplus="13";
         }
        if (scintnum==13)
        {
        scint="13";
        scintplus="14";
        }
        if (scintnum==14)
        {
        scint="14";
        scintplus="15";
        }
        if (scintnum==15)
          {
        scint="15";
        scintplus="16";
        }
        if (scintnum==16)
        {
        scint="16";
        scintplus="01";
        }

        c1.cd(n);
        TObject *obj;
        obj = ana.GetNext();

      ana.Plot(octant+scint+"fra>>"+ana.fCurrentString.Data(),octant+sc
      int+"frt>0&&"+octant+scint+"flt>0&&"+octant+scint+"brt>0&&"+octan
      t+scint+"blt>0&&"+octant+scintplus+"brt>0");
      TH1F* hist1 = (TH1F*)gROOT-
>FindObject(ana.fCurrentString.Data());
      TF1* fit = new TF1("fit","landau");
      hist1->Fit("fit");
      hist1->GetXaxis()->SetTitle("Amplitude");
      hist1->GetXaxis()->CenterTitle();
      hist1->GetYaxis()->SetTitle("Number of Events");
      hist1->GetYaxis()->CenterTitle();
      hist1->SetTitle(run+" "+octant+scint+"fra"+" ADC when TDC hit");
      n=n+1;
```

```
hist1->GetFunction("landau");
mean =fit->GetParameter(1);
emean=fit->GetParError(1);
sigma=fit->GetParameter(2);
esigma=fit->GetParError(2);
histogram=octant+scint+"fra";
DataFile<<run<<"    "<<histogram<<"     ";
DataFile<<mean<<"        "<<emean<<"         "<<sigma<<"
"<<esigma<<"\n";

c1.cd(n);
ana.GetNext();

ana.Plot(octant+scint+"fla>>"+ana.fCurrentString.Data(),octant+sc
int+"flt>0&&"+octant+scint+"frt>0&&"+octant+scint+"brt>0&&"+octan
t+scint+"blt>0&&"+octant+scintplus+"brt>0");
TH1F* hist2 = (TH1F*)gROOT-
>FindObject(ana.fCurrentString.Data());
TF1* fit = new TF1("fit","landau");
hist2->Fit("fit");
hist2.Fit("landau");
hist2->GetXaxis()->SetTitle("Amplitude");
hist2->GetXaxis()->CenterTitle();
hist2->GetYaxis()->SetTitle("Number of Events");
hist2->GetYaxis()->CenterTitle();
hist2->SetTitle(run+" "+octant+scint+"fla"+" ADC when TDC hit");
n=n+1;
hist2->GetFunction("landau");
mean =fit->GetParameter(1);
emean=fit->GetParError(1);
sigma=fit->GetParameter(2);
esigma=fit->GetParError(2);
histogram=octant+scint+"fla";
DataFile<<run<<"    "<<histogram<<"     ";
DataFile<<mean<<"        "<<emean<<"         "<<sigma<<"
"<<esigma<<"\n";

c1.cd(n);
ana.GetNext();

ana.Plot(octant+scint+"bra>>"+ana.fCurrentString.Data(),+octant+s
cint+"brt>0&&"+octant+scint+"blt>0&&"+octant+scint+"frt>0&&"+octa
nt+scint+"flt>0&&"+octant+scintplus+"brt>0");
TH1F* hist3 = (TH1F*)gROOT-
>FindObject(ana.fCurrentString.Data());
TF1* fit = new TF1("fit","landau");
hist3->Fit("fit");
hist3.Fit("landau");
hist3->GetXaxis()->SetTitle("Amplitude");
hist3->GetXaxis()->CenterTitle();
hist3->GetYaxis()->SetTitle("Number of Events");
hist3->GetYaxis()->CenterTitle();
hist3->SetTitle(run+" "+octant+scint+"bra"+" ADC when TDC hit");
n=n+1;
hist3->GetFunction("landau");
mean =fit->GetParameter(1);
emean=fit->GetParError(1);
```

```
        sigma=fit->GetParameter(2);
        esigma=fit->GetParError(2);
        histogram=octant+scint+"bra";
        DataFile<<run<<"   "<<histogram<<"    ";
        DataFile<<mean<<"       "<<emean<<"        "<<sigma<<"
        "<<esigma<<"\n";
        c1.cd(n);
        ana.GetNext();

        ana.Plot(octant+scint+"bla>>"+ana.fCurrentString.Data(),+octant+s
        cint+"blt>0&&"+octant+scint+"brt>0&&"+octant+scint+"flt>0&&"+octa
        nt+scint+"frt>0&&"+octant+scintplus+"brt>0");
        TH1F* hist4 = (TH1F*)gROOT-
>FindObject(ana.fCurrentString.Data());
        TF1* fit = new TF1("fit","landau");
        hist4->Fit("fit");
        hist4.Fit("landau");
        hist4->GetXaxis()->SetTitle("Amplitude");
        hist4->GetXaxis()->CenterTitle();
        hist4->GetYaxis()->SetTitle("Number of Events");
        hist4->GetYaxis()->CenterTitle();
        hist4->SetTitle(run+" "+octant+scint+"bla"+" ADC when TDC hit");
        n=n+1;
        hist4->GetFunction("landau");
        mean =fit->GetParameter(1);
        emean=fit->GetParError(1);
        sigma=fit->GetParameter(2);
        esigma=fit->GetParError(2);
        histogram=octant+scint+"bla";
        DataFile<<run<<"   "<<histogram<<"    ";
        DataFile<<mean<<"       "<<emean<<"        "<<sigma<<"
        "<<esigma<<"\n";

        scintnum=scintnum+1;

        }

      n=1;

      c1.Update();
      ps->NewPage();
      c1.Clear();
      c1.Divide(2,2);

    }

      scintnum=1;

  }

//DataFile.close();
ps->Close();

}
```

Bibliography

[1]   K.A. Anion *et al.,* Phys. Rev. Lett. 82, 1096 (1999).

[2]   D.T. Spayde *et al*., Phys. Rev. Lett. 78, 3824 (1997).

[3]   *PAC Jeopardy Proposal G^0 Experiment (originally E91-017)*, (1998), (unpublished).

[4]   I. S. Hughes, *Elementary Particles*, Cambridge University Press, Cambridge, (1991).

[5]   Donald H. Perkins, *Introduction to High Energy Physics*, (Addison-Wesley Publishing Company Inc., California, 1987).

[6]   Samuel S.S. Wong, *Introductory Nuclear Physics,* (Prentice-Hall Inc., New Jersey, 1990).

[7]   Knoll, Glen F., *Radiation Detection and Measurement,* (John Wiley & Sons, Inc. New York, 2000).

[8]   Rene Brun/CERN *et al.*, *ROOT Users Guide 3.1c*, (2001), (unpublished).